ALMA MATER STUDIORUM - UNIVERSITÀ DI BOLOGNA

FACOLTA' DI INGEGNERIA

CORSO DI LAUREA IN INGEGNERIA CIVILE

DISTART

Dipartimento di Ingegneria delle Strutture, dei Trasporti, delle Acque, del Rilevamento, del Territorio

TESI DI LAUREA

in

Calcolo Automatico delle Strutture

A NEW INSIGHT IN STRESS RECOVERY TECHNIQUES AND HESSIAN RECONSTRUCTION METHODS

CANDIDATO

Luca Patruno

RELATORE

Prof. Francesco Ubertini

CORRELATORE

Dott. Ing. Stefano de Miranda

Ing. Alejandro Gutierrez

Anno Accademico 2009/2010

Sessione II

Sommario

Le tecniche di ricostruzione degli sforzi sono state un campo di ricerca attivo sin dal 1987, quando Zienkiewicz e Zhu hanno proposto una procedura chiamata Superconvergent Patch Recovery (SPR) [1]. Tale procedura si basa su un'interpolazione ai minimi quadrati degli sforzi in punti superconvergenti su raggruppamenti di elementi contigui chiamati patch e fornisce campi di sforzo accurati che possono essere usati per stimare l'errore di discretizzazione. Negli anni seguenti sono state proposte numerose varianti di questa procedura cercando di migliorarne le prestazioni aggiungendo il soddisfacimento delle condizioni d'equilibrio. Successivamente è stata proposta un'altra tecnica chiamata Recovery by Equilibrium in Patches (REP) [2]. In questo caso l'idea consiste nell'imporre l'equilibrio in forma debole su patch di elementi e risolvere le equazioni risultanti secondo uno schema ai minimi quadrati.

Più recentemente è stata proposta un'altra procedura, basata sulla minimizzazione dell'energia complementare, chiamata Recovery by Compatibility in Patches (RCP) [3]. Questa procedura, per certi versi, può essere considerata la versione duale della REP poiché, sostanzialmente, impone la compatibilità in forma debole proiettando gli sforzi su un set di modi autoequilibrati.

In questa tesi è presentata una forma migliorata dell'RCP allo scopo di garantire la convergenza delle derivate seconde delle risultanti degli sforzi. Al fine di ottenere tale risultato sono state testate due diverse strategie e la loro combinazione. La prima è di considerare patch più estese secondo quanto proposto in [4] mentre la seconda consiste nell'effettuare una seconda ricostruzione sugli sforzi ricostruiti. Si presentano alcuni test numerici effettuati in stato piano di tensione al fine di verificare e confrontare l'efficacia delle diverse procedure.

Successivamente, una nuova tecnica di recovery chiamata Last Square Displacements (LSD) è presentata. La nuova procedura si basa sull'interpolazione secondo uno schema ai minimi quadrati degli spostamenti nodali ottenuti dall'analisi agli elementi finiti. Si è infatti osservato che la maggior parte dell'errore associato alle risultanti degli sforzi è introdotto nel momento in cui le funzioni di forma sono derivate per ottenere le deformazioni a partire degli spostamenti nodali.

Questa procedura si è mostrata essere ultraconvergente ed è estremamente efficiente in quanto necessita in input solo degli spostamenti nodali che sono ottenuti direttamente dalla soluzione agli elementi finiti, evitando di dover estrarre i valori della risultante degli sforzi con il metodo tradizionale. Vengono dunque presentati alcuni test numerici in caso di stato piano di tensione che mostrano che la procedura è ultraconvergente e garantisce la convergenza delle derivate prime e seconde delle risultanti degli sforzi.

Infine si presenta la ricostruzione degli sforzi trasversali nell'ambito della First-order Shear Deformation Theory nel caso delle piastre laminate mediante l'uso delle equazioni indefinite d'equilibrio tridimensionali. Si può dimostrare che [5] la convergenza di tale strategia di ricostruzione dipende dalla convergenza delle derivate prime e seconde delle risultanti degli sforzi che non è a priori garantita dalla maggior parte degli elementi finiti di basso ordine. RCP e LSD sono dunque qui usate al fine di garantire tale convergenza assicurando anche quella degli sforzi ricostruiti. Si presentano, in fine, test numerici che confermano la validità di entrambe le procedure.

Index

Introduction

Stress recovery techniques have been an active research topic in the last few years since, in 1987, Zienkiewicz and Zhu proposed a procedure called Superconvergent Patch Recovery (SPR) [1]. This procedure is a last-squares fit of stresses at super-convergent points over patches of elements and it leads to enhanced stress fields that can be used for evaluating finite element discretization errors. In subsequent years, numerous improved forms of this procedure have been proposed attempting to add equilibrium constraints to improve its performances. Later, another superconvergent technique, called Recovery by Equilibrium in Patches (REP), has been proposed in [2]. In this case the idea is to impose equilibrium in a weak form over patches and solve the resultant equations by a last-square scheme.

In recent years another procedure, based on minimization of complementary energy, called Recovery by Compatibility in Patches (RCP) has been proposed in [3]. This procedure, in many ways, can be seen as the dual form of REP as it substantially imposes compatibility in a weak form among a set of self-equilibrated stress fields.

In this thesis a new insight in RCP is presented and the procedure is improved aiming at obtaining convergent second order derivatives of the stress resultants. In order to achieve this result, two different strategies and their combination have been tested. The first one is to consider larger patches in the spirit of what proposed in [4] and the second one is to perform a second recovery on the recovered stresses. Some numerical tests in plane stress conditions are presented, showing the effectiveness of these procedures.

Afterwards, a new recovery technique called Last Square Displacements (LSD) is introduced. This new procedure is based on last square interpolation of nodal displacements resulting from the finite element solution. In fact, it has been observed that the major part of the error affecting stress resultants is introduced when shape functions are derived in order to obtain strains components from displacements.

This procedure shows to be ultraconvergent and is extremely cost effective, as it needs in input only nodal displacements directly coming from finite element solution, avoiding any other post-processing in order to obtain stress resultants using the traditional method. Numerical tests in plane stress conditions are than presented showing that the procedure is ultraconvergent and leads to convergent first and second order derivatives of stress resultants.

In the end, transverse stress profiles reconstruction using First-order Shear Deformation Theory for laminated plates and three dimensional equilibrium equations is presented. It can be seen [5] that accuracy of this reconstruction depends on accuracy of first and second derivatives of stress resultants, which is not guaranteed by most of available low order plate finite elements. RCP and LSD procedures are than used to compute convergent first and second order derivatives of stress resultants ensuring convergence of reconstructed transverse shear and normal stress profiles respectively. Numerical tests are presented and discussed showing the effectiveness of both procedures.

Chapter 1

First-order Shear Deformation Theory (FSDT)

For further convenience FSDT is here introduced so that in subsequent sections, stress recovery techniques will be presented for this structural model that will constitute the theoretical base for stress profile reconstruction presented in Chapter 8.

First-order Shear Deformation Theory is here extended to laminated plates and presented as a two dimensional theory directly descending from a three dimensional one. This allows to rationally justify the introduction of the shear correction factor in the finite element solution and the use of three dimensional equilibrium equations for the reconstruction strategy of transverse stresses.

Consider a flat cylinder with cross-section Ω and constant thickness h is:

$$\mathcal{C} = \left\{ (x,y,z) \in \mathbb{R}^3 \middle| z \in \left(-\frac{h}{2}, \frac{h}{2} \right), (x,y) \in \Omega \subset \mathbb{R}^2 \right\} \tag{1.1}$$

The classical Reissner–Mindlin kinematic assumptions for shearable plates are applied to a multilayered structure considering the displacement field defined as:

$$\boldsymbol{d} = \begin{bmatrix} \boldsymbol{u} + z\boldsymbol{\vartheta} \\ w \end{bmatrix} \tag{1.2}$$

being $\boldsymbol{u}$ a vector of in-plane displacements and $\boldsymbol{\vartheta}$ a vector containing rotations of the fibre, orientated in the z direction, with respect to its undeformed configuration.

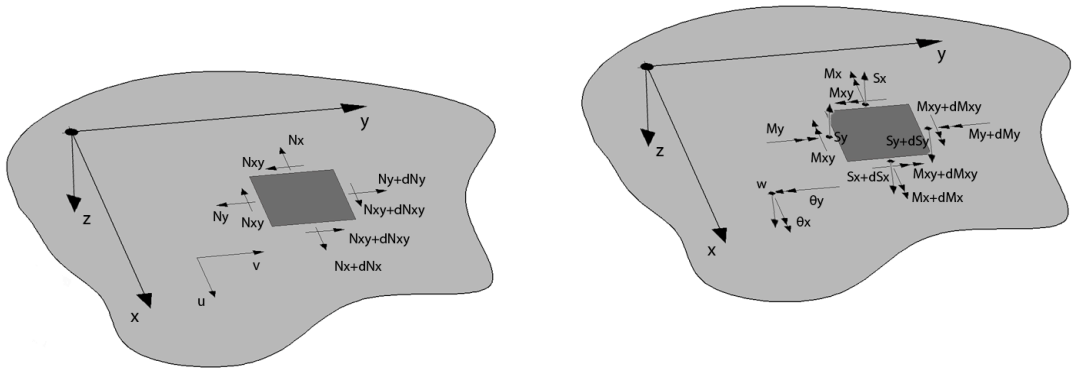

Fig 2.1 – Kinematic and static plate quantities

Using these kinematic assumptions, punctual strains in the three dimensional domain can be derived from the following compatibility equations:

$$\boldsymbol{e} = \boldsymbol{D}_p\boldsymbol{u} + z\boldsymbol{D}_b\boldsymbol{\vartheta} = \boldsymbol{\mu} + z\boldsymbol{\chi} \tag{1.3}$$

$$\boldsymbol{\gamma} = \boldsymbol{D}_s w + \boldsymbol{\vartheta} \tag{1.4}$$

where $\boldsymbol{e}$ and $\boldsymbol{\gamma}$ are in-plane and transverse three dimensional strain vectors respectively, $\boldsymbol{\mu}$ is a vector of in-plane strains and $\boldsymbol{\chi}$ is a vector of curvatures. The mentioned first-order differential operators can be written as:

$$\boldsymbol{D}_p = \boldsymbol{D}_b = \begin{bmatrix} \dfrac{\partial}{\partial x} & 0 \\ 0 & \dfrac{\partial}{\partial y} \\ \dfrac{\partial}{\partial y} & \dfrac{\partial}{\partial x} \end{bmatrix}, \qquad \boldsymbol{D}_s = \begin{bmatrix} \dfrac{\partial}{\partial x} \\ \dfrac{\partial}{\partial y} \end{bmatrix} \tag{1.5}$$

so that compatibility equations are:

$$\boldsymbol{\mu} = \boldsymbol{D}_p\boldsymbol{u}\,, \qquad \boldsymbol{\chi} = \boldsymbol{D}_b\boldsymbol{\vartheta}\,, \qquad \boldsymbol{\gamma} = \boldsymbol{D}_s w + \boldsymbol{\vartheta} \tag{1.6}$$

Equilibrium equations can be obtained through the principle of virtual work in the form:

$$\boldsymbol{D}_p^* \boldsymbol{N} = \boldsymbol{q}_x \,, \qquad \boldsymbol{D}_b^* \boldsymbol{M} + \boldsymbol{S} = \boldsymbol{c} \,, \qquad \boldsymbol{D}_s^* \boldsymbol{S} = q_z \tag{1.7}$$

being $\boldsymbol{N}$, $\boldsymbol{M}$ and $\boldsymbol{S}$ the membrane stress resultants, the moments and the shear stress resultants respectively, $\boldsymbol{q}_x$ the in plane load vector, $\boldsymbol{c}$ the distributed couples vector, q_z the transverse load and $\boldsymbol{D}_p^*$, $\boldsymbol{D}_b^*$ and $\boldsymbol{D}_s^*$ first order differential operators, adjoint to $\boldsymbol{D}_p$, $\boldsymbol{D}_b$ and $\boldsymbol{D}_s$, respectively.

Stress resultants are defined as:

$$\boldsymbol{N} = \int_{-\boldsymbol{h}/2}^{\boldsymbol{h}/2} \boldsymbol{s} dz \,, \qquad \boldsymbol{M} = \int_{-\boldsymbol{h}/2}^{\boldsymbol{h}/2} z \boldsymbol{s} dz \,, \qquad \boldsymbol{S} = \int_{-\boldsymbol{h}/2}^{\boldsymbol{h}/2} \boldsymbol{\tau} dz \tag{1.8}$$

Finally constitutive equation are given by:

$$\boldsymbol{N} = \boldsymbol{C}_m \boldsymbol{\mu} + \boldsymbol{C}_{mb} \boldsymbol{\chi} \,, \qquad \boldsymbol{M} = \boldsymbol{C}_{mb} \boldsymbol{\mu} + \boldsymbol{C}_b \boldsymbol{\chi} \,, \qquad \boldsymbol{S} = \boldsymbol{C}_s \boldsymbol{\gamma} \tag{1.9}$$

where $\boldsymbol{C}_m$, $\boldsymbol{C}_{mb}$, $\boldsymbol{C}_b$ and $\boldsymbol{C}_s$, in case of a laminated plate composed of superimposed homogenous layers, are defined as follows:

$$\boldsymbol{C}_m = \sum_{k=1}^{n.layers} \left(z_k - z_{k-1}\right) \boldsymbol{C}_m^{(k)} \,, \qquad \boldsymbol{C}_{mb} = \frac{1}{2} \sum_{k=1}^{n.layers} \left(z_k^2 - z_{k-1}^2\right) \boldsymbol{C}_m^{(k)}$$

$$\boldsymbol{C}_b = \frac{1}{3} \sum_{k=1}^{n.layers} \left(z_k^3 - z_{k-1}^3\right) \boldsymbol{C}_m^{(k)} \,, \qquad \boldsymbol{C}_s = \boldsymbol{k} \odot \sum_{k=1}^{n.layers} \left(z_k - z_{k-1}\right) \boldsymbol{C}_s^{(k)} \tag{1.10}$$

In the preceding relations z_k and z_{k-1} are the top and bottom coordinates of the k-*th* lamina, $\boldsymbol{C}_m^{(k)}$ and $\boldsymbol{C}_s^{(k)}$ are its constitutive matrix and $\boldsymbol{k}$ is 2x2 matrix containing shear correction factors while $\odot$ operator denotes the component by component product. For every single layer it is therefore possible to write:

$$\boldsymbol{s} = \boldsymbol{C}_m^{(k)} \boldsymbol{e} \,, \qquad \boldsymbol{\tau} = \boldsymbol{k} \odot \boldsymbol{C}_s^{(k)} \boldsymbol{\gamma} \tag{1.11}$$

Chapter 2

Recovery by Compatibility in Patches

Recovery by Compatibility in Patches has been early proposed in [3] and extended to homogenous plates in [6]. The idea is to obtain recovered stresses resultants by minimizing the complementary energy associated to a patch of elements, considered as a separate system, among an assumed set of self-equilibrated stress fields. Hence, it substantially attempts to enhance equilibrium while relaxing compatibility.

Patches can be created considering a node or an element (Fig 2.1) and then adding as many orders of adjacent elements as needed in order to reach the required size.

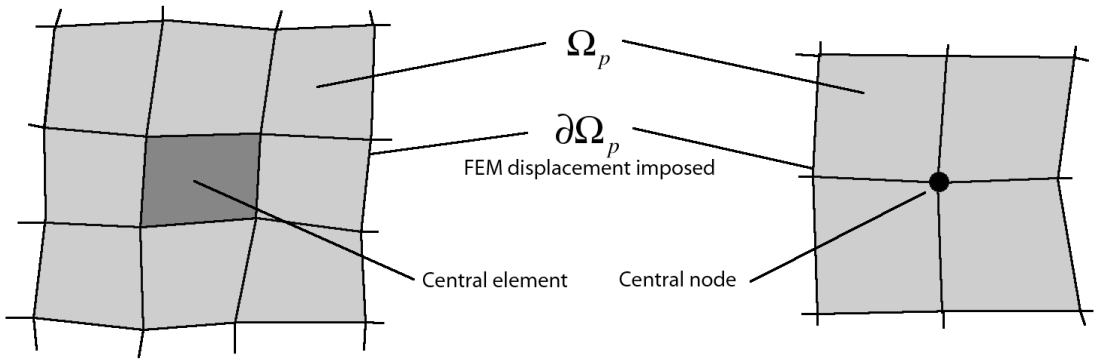

(a) (b)

Fig 2.1 – Element patch (a); Node Patch (b)

In other works [5], the patch creation procedure was driven by the number of hems that were created around the element or the node. In this case, instead, hems are added until a minimum number of included elements is reached, typically equal to the one enclosed in the free field patch (Fig 2.2). Using this patch creation method, boundary patches have at least the same number of elements of the free field patch ensuring stability of the procedure at the border.

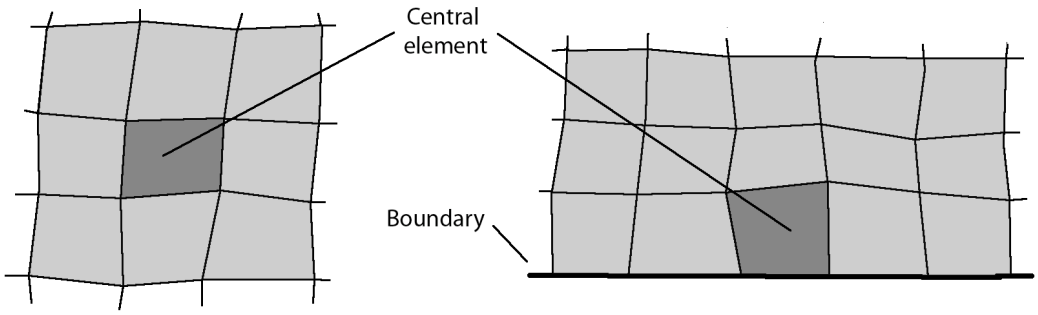

(a) (b)

Fig 2.2 – Free field patch (a); Boundary patch (b)

If patches are centred on nodes the result is a node-patch while, if elements are chosen as central entity, element-patches are obtained. In the first case, once reconstructed stress fields are derived by RCP minimization, in the element domain the reconstructed solution is obtained averaging the values coming from all the considered element's nodes directly in the point of interest (Fig 2.3). This strategy, differently from other procedures that compute the reconstructed stress fields using nodal values and shape functions, leads to pointwise equilibrated stress fields that are discontinuous between elements.

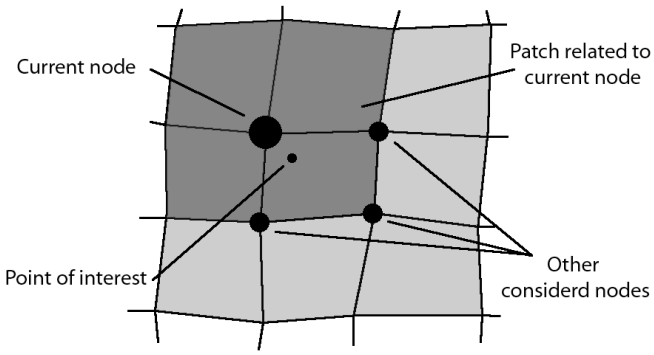

Fig 2.3 – Stress field extraction for node patch.

In the second case the reconstructed stress fields on the patch is directly taken as the reconstructed solution for the central element so that no averaging process is needed. If this stress extraction strategies are adopted, no relevant difference between node-patch and element-patch performances have been observed being the major difference the number of element in the free field patch.

To apply the recovery procedure, a new approximation for stress resultants over the patch is introduced:

$$\begin{bmatrix} \boldsymbol{N}^r \\ \boldsymbol{M}^r \\ \boldsymbol{S}^r \end{bmatrix} = \boldsymbol{P}^r \boldsymbol{\alpha} + \begin{bmatrix} \boldsymbol{N}_p \\ \boldsymbol{M}_p \\ \boldsymbol{S}_p \end{bmatrix} \tag{2.1}$$

where the superscript *r* denotes the recovered solution, P^r is a matrix reporting on columns a set of self equilibrated modes, $\boldsymbol{\alpha}$ is a vector of unknown parameters and $\left(\boldsymbol{N}_p, \boldsymbol{M}_p, \boldsymbol{S}_p\right)$ is a particular solution of the plate equilibrium equations depending on external loads.

Then the RCP minimization yields to the following compatibility condition over each patch if First-order Shear Deformation Theory is chosen as structural model:

$$\int_{\Omega_p} \left[\delta \boldsymbol{N}^{rT} \left(\boldsymbol{\mu}^r - \boldsymbol{\mu}^h \right) + \delta \boldsymbol{M}^{rT} \left(\boldsymbol{\chi}^r - \boldsymbol{\chi}^h \right) + \delta \boldsymbol{S}^{rT} \left(\boldsymbol{\gamma}^r - \boldsymbol{\gamma}^h \right) \right] d\Omega_p \quad \forall \left(\delta \boldsymbol{N}^r, \delta \boldsymbol{M}^r, \delta \boldsymbol{S}^r \right) \tag{2.2}$$

where Ω_p is the patch domain, $\left(\boldsymbol{\mu}^r,\ \boldsymbol{\chi}^r,\ \boldsymbol{\gamma}^r\right)$ are the strain components obtained by the recovered stress resultants via the plates constitutive equations and $\left(\boldsymbol{\mu}^h,\ \boldsymbol{\chi}^h,\ \boldsymbol{\gamma}^h\right)$ are the strain components resulting from the finite element solution.

In all subsequent developments, a complete set of quadratic self-equilibrated stress modes have been chosen so that it is possible to directly evaluate second order derivatives of stress resultants simply considering analytic derivatives of the modes and the particular solution.

Substituting equation (2.1) in (2.2) leads to a system of linear algebraic equations, whose solution permits to determinate parameter α and, consequently, the recovered stress field over the patch:

$$\boldsymbol{H}\boldsymbol{\alpha} = \boldsymbol{g} \tag{2.3}$$

where

$$\boldsymbol{H} = \sum_{j=1}^{nep} \int_{\Omega_j} \left(\boldsymbol{P}^{rT} \boldsymbol{C}^{-1} \boldsymbol{P}^{r} \right) d\Omega_j \,, \quad \boldsymbol{g} = \sum_{j=1}^{nep} \int_{\Omega_j} \left(\boldsymbol{P}^{rT} \left(\boldsymbol{\mu}^{h}, \boldsymbol{\chi}^{h}, \boldsymbol{\gamma}^{h} \right) - \boldsymbol{P}^{rT} \boldsymbol{C}^{-1} \left(\boldsymbol{N}^{p}, \boldsymbol{M}^{p}, \boldsymbol{S}^{p} \right) \right) d\Omega_j \tag{2.4}$$

being nep the number of element in the patch, Ω_j the generic element domain, and C^{-1} the inverse of the plate constitutive matrix.

Considering for simplicity a linear polynomial expansion instead of a quadratic one, (2.1) can be written as:

$$\begin{bmatrix} N_x^r \\ N_y^r \\ N_{xy}^r \\ M_x^r \\ M_y^r \\ M_{xy}^r \\ S_x^r \\ S_y^r \end{bmatrix} = \begin{bmatrix} 1 & 0 & 0 & y & 0 & x & 0 & 0 & 0 & 0 & 0 & 0 & 0 & 0 & 0 & 0 \\ 0 & 1 & 0 & 0 & x & 0 & y & 0 & 0 & 0 & 0 & 0 & 0 & 0 & 0 & 0 \\ 0 & 0 & 1 & 0 & 0 & -y & -x & 0 & 0 & 0 & 0 & 0 & 0 & 0 & 0 & 0 \\ 0 & 0 & 0 & 0 & 0 & 0 & 0 & 1 & 0 & 0 & x & y & 0 & 0 & 0 & 0 \\ 0 & 0 & 0 & 0 & 0 & 0 & 0 & 0 & 1 & 0 & 0 & 0 & x & y & 0 & 0 \\ 0 & 0 & 0 & 0 & 0 & 0 & 0 & 0 & 0 & 1 & 0 & 0 & 0 & 0 & y & x \\ 0 & 0 & 0 & 0 & 0 & 0 & 0 & 0 & 0 & 0 & 1 & 0 & 0 & 0 & 1 & 0 \\ 0 & 0 & 0 & 0 & 0 & 0 & 0 & 0 & 0 & 0 & 0 & 0 & 0 & 1 & 0 & 1 \end{bmatrix} \boldsymbol{\alpha} + \begin{bmatrix} N_x^p \\ N_y^p \\ N_{xy}^p \\ M_x^p \\ M_y^p \\ M_{xy}^p \\ S_x^p \\ S_y^p \end{bmatrix} \tag{2.5}$$

where

$$\begin{bmatrix} N_x^p \\ N_y^p \\ N_{xy}^p \end{bmatrix} = \begin{bmatrix} -\int_0^x q_x \, dx \\ -\int_0^y q_y \, dy \\ 0 \end{bmatrix}, \quad \begin{bmatrix} M_x^p \\ M_y^p \\ M_{xy}^p \end{bmatrix} = \begin{bmatrix} \int_0^x (S_{xp} - c_x) dx \\ \int_0^y (S_{yp} - c_y) dy \\ 0 \end{bmatrix}, \quad \begin{bmatrix} S_x^p \\ S_y^p \end{bmatrix} = -\frac{1}{2} \begin{bmatrix} \int_0^x q_z \, dx \\ \int_0^y q_z \, dy \end{bmatrix} \tag{2.7}$$

being $\left[q_x, q_y, q_z \right]$ distributed surface load and $\left[c_x, c_y \right]$ distributed couples.

In order to guarantee convergence of second order derivatives of stress resultants, two different strategies and their combination are here proposed. The first one is to consider wider patches (Fig 2.4) and the second one is to perform a second recovery on the recovered stresses. This is possible obtaining, through constitutive equations, strains related to recovered stresses and using them in a second recovery procedure. Four procedures are then analyzed:

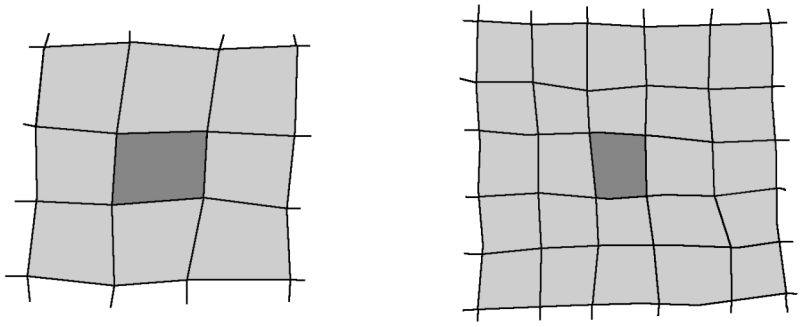

(a) (b)

Fig 2.4 –Patch type A (a), Patch type B (b).

Type 1 - Single RCP on patch type A
Type 2 - Single RCP on patch type B
Type 3 - Double RCP on patch type A
Type 4 - Double RCP on patch type B

where Type 1 corresponds to the RCP in its standard form [3], used in [5] in order to obtain convergence of first derivatives in a laminated plate bending problem with the only difference that in that case standard patch creation method was adopted so that boundary patches were smaller than free field ones.

Chapter 3

Numerical results presentation

In the next chapter the four proposed procedures are tested on plain stress benchmark problems. In order to adapt the formulation obtained for RCP considering a FSDT structural model, it is sufficient to consider equal to zero all the quantities related to shear and bending effects and impose the constitutive equations for plain stress problems to membrane strains and stress resultants. In order to avoid singularity of constitutive matrix the diagonal elements outside the membrane related submatrix can be taken equal to unity and anyway different from zero.

Benchmark problem require that analytical solution is known so that error associated to numerical solution can be calculated. In this case a displacement field has been supposed over the considered domain. Analytical stress resultants fields can be calculated substituting compatibility equations (1.6) into the constitutive equations (1.9). Then, using equilibrium equations (1.7), analytical load fields can be obtained.

The problem is then solved using a Finite Element approach in with analytical displacements are imposed at the domain boundary nodes and the load fields are applied in the domain.

A unit length square domain is considered. Thickness is supposed to be equal to one tenth of the side length. Elastic modulus is 1000000 and Poisson modulus equal to 0.3.

Analytic displacements fields for benchmark problems are here presented:

Problem 1 - $u = xy\sin(\pi x)\sin(\pi y)$

Problem 2 - $u = xy(1-x)(1-y)(1+2x+7y)$

Problem 3 - $u = y^3$

In order to evaluate the effectiveness and the performances of the procedures, error convergence rate is calculated. This quantity is defined in different ways depending on the physical meaning of the investigated quantity. In particular, if stress resultants are considered, error is calculated in energy norm resulting for membrane problems in:

$$e = \frac{1}{2}(\boldsymbol{N} - \boldsymbol{N}_{ex})^T \boldsymbol{C}^{-1}(\boldsymbol{N} - \boldsymbol{N}_{ex}) \tag{3.1}$$

where $\boldsymbol{N}$ is the vector of numerically calculated membrane stress resultants, $\boldsymbol{N}_{ex}$ is the analytical solution and $\boldsymbol{C}^{-1}$ is the inverse of the constitutive matrix.

When stress resultants derivatives are considered, energy norm has not precise physical meaning so that a scalar product is preferred:

$$e = (\boldsymbol{dN} - \boldsymbol{dN}_{ex})^T (\boldsymbol{dN} - \boldsymbol{dN}_{ex}) \tag{3.2}$$

where $\boldsymbol{dN}$ is a column vector containing for each stress resultant its derivative in both axis directions and for second derivatives also the mixed one.

Since all defined error indicators are related to the quadratic value of stress resultants errors, in all subsequent results error is considered as the square root of the quantity just defined.

Global convergence is then evaluated integrating the error in the whole domain and comparing it with mesh refinements in a double logarithmic graph.

Global convergence is a key synthetic indicator to evaluate the effectiveness of the procedures. Nevertheless to have a deeper understanding of its behaviour, in this thesis a new representation of this data is developed. The idea is that if mesh refinements are performed dividing each element in more elements, the original element nodes are

common to the finer and the coarser mesh. This means that convergence maps can be created locally comparing the error variation estimated like in (3.1) and (3.2) and the variation of the characteristic mesh length. Since reconstructed stress fields are discontinuous between elements, error associated to the point is calculated averaging all values obtained considering the node as part of all its adjacent elements. This maps permits to directly observe the presence of super-convergent points and check the procedure's stability at boundary patches.

Another important evaluation instrument are accuracy maps. In this thesis they are obtained representing the local error associated to a point and then dividing it for the maximum value of the related local energy found in the domain. In order to render the results in a clearer way the logarithm is then extracted.

In subsequent chapters, stress resultants accuracy maps are obtained considering an internal mesh of 3x3 gauss points in the element domain plus their projection on the element sides for each element.

All subsequent results have been obtained considering four node elements on regular mesh and refinements obtained dividing each side with 8, 16, 32 and 64 elements.

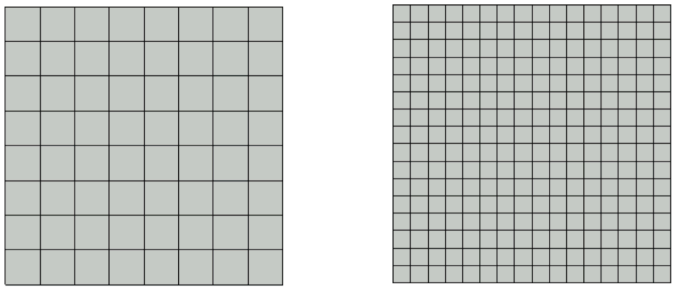

(a) (b)

Fig 3.1 – 8 (a) and 16 (b) elements per side mesh refinements

Chapter 4

Numerical tests for RCP

Problem 1

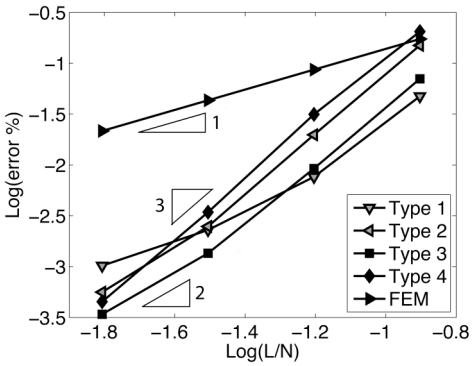

(a)

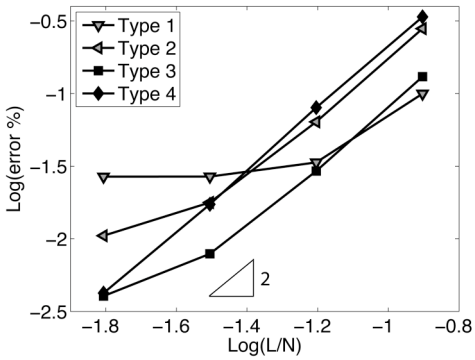

(b)

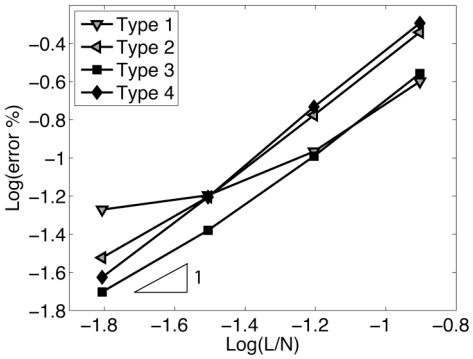

(c)

Fig 4.1 – Global convergence of stresses (a), first derivatives (b), second derivatives (c)

Subsequent accuracy maps are obtained on a 64 elements per side mesh and convergence maps are obtained comparing error associated to 32 and 64 elements per side refinements.

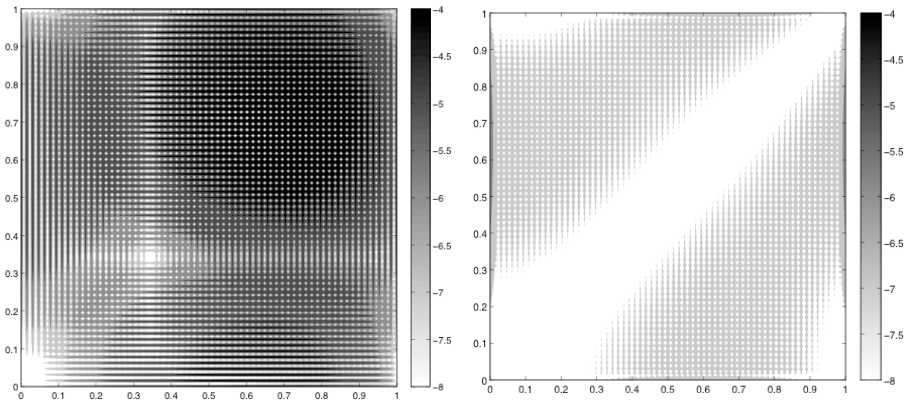

(a) (b)

Fig 4.1 – Accuracy maps. Finite element (a), RCP Type 1 (b)

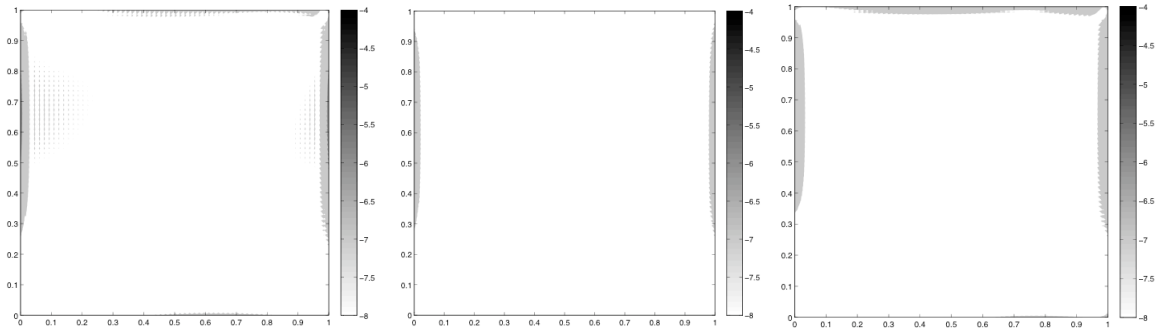

(a) (b) (c)

Fig 4.2 – Accuracy maps. RCP Type 2 (a), RCP Type 3 (b), RCP Type 4 (c)

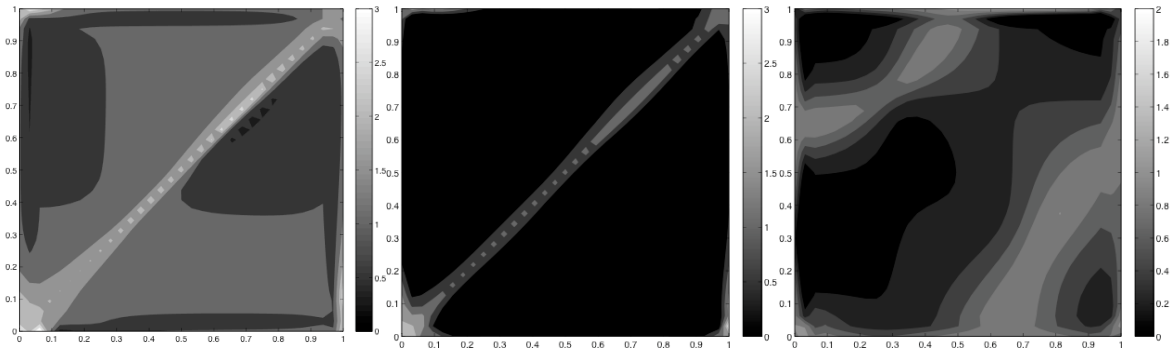

(a) (b) (c)

Fig 4.3 – Convergence maps of RCP Type 1. Stresses (a), First derivatives (b), Second derivatives (c)

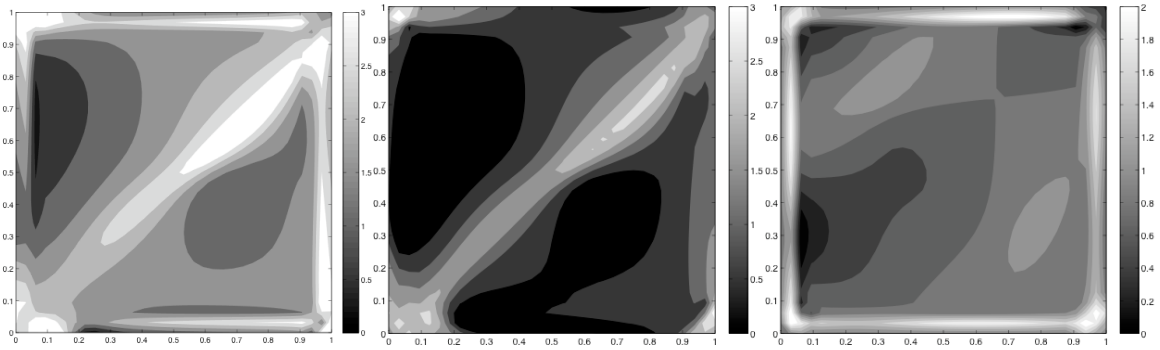

(a) (b) (c)

Fig 4.4 – Convergence maps of RCP Type 2. Stresses (a), First derivatives (b), Second derivatives (c)

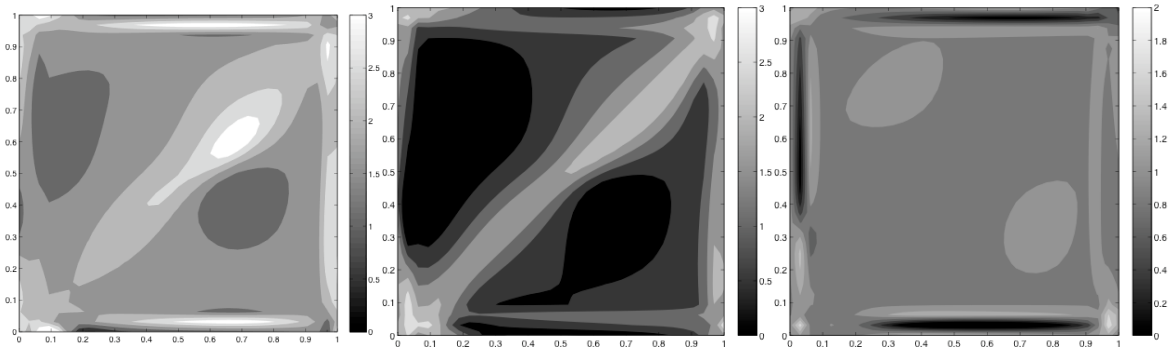

(a) (b) (c)

Fig 4.5 – Convergence maps of RCP Type 3. Stresses (a), First derivatives (b), Second derivatives (c)

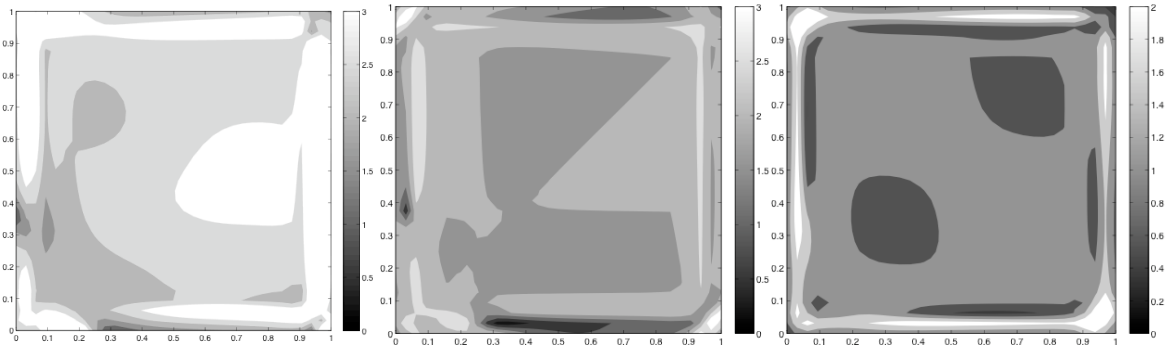

(a) (b) (c)

Fig 4.9 – Convergence maps of RCP Type 4. Stresses (a), First derivatives (b), Second derivatives (c)

It can be observed that, contrarily from what was expected, in this test RCP seems to have better asymptotical stability in evaluating second derivatives than first derivatives. Considering problems with polynomial analytical solution it has been possible to understand that RCP is affected by random activation of low order modes due to discretization errors in finite element solution. The contribution of these modes is modest but when high accuracy are reached, they become dominant. This explains why, in some cases, second derivatives shows higher stability than first ones. It has been proven that the problem can be corrected under-integrating complementary energy using a single Gauss point. Doing so the procedure becomes very similar to SPR with equilibrium constraints but physical meaning is lost.

It is well known that in finite element solution, some point in the element domain are characterized by great accuracy and superconvergence. Starting from this observation in 1987 Zienkiewicz and Zhu [1] proposed SPR that, as already mentioned, is a recovery technique based on interpolation of stresses at optimal stress points. Subsequent accuracy maps, together with Fig 4.1 (a), show that the centre of the element is characterized by accuracy that can be two and more order of magnitude higher than the rest of the element domain, confirming the validity of the idea beneath SPR procedure.

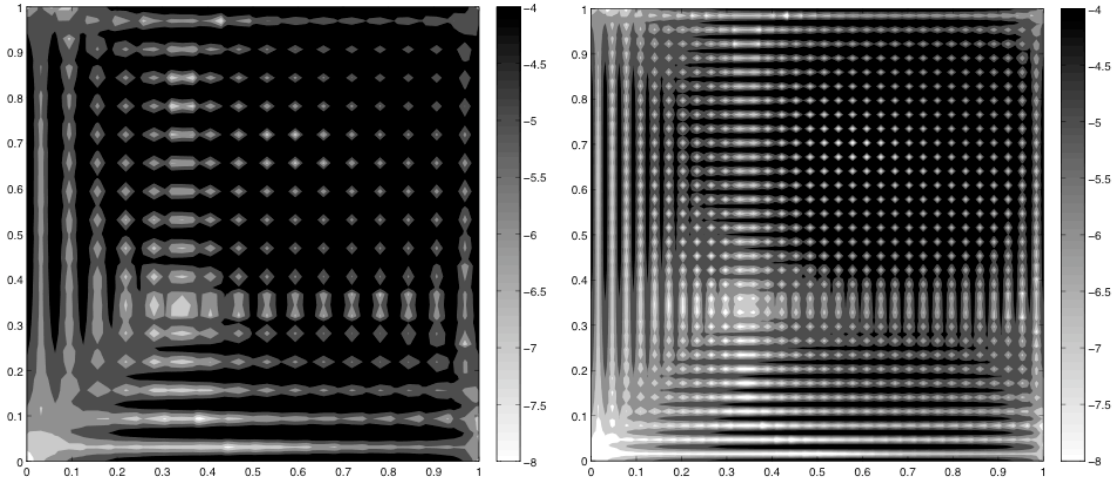

(a) (b)

Fig 4.10 – Accuracy maps of Fem stresses for 16 (a) and 32 (b) elements per side meshes

Problem 2

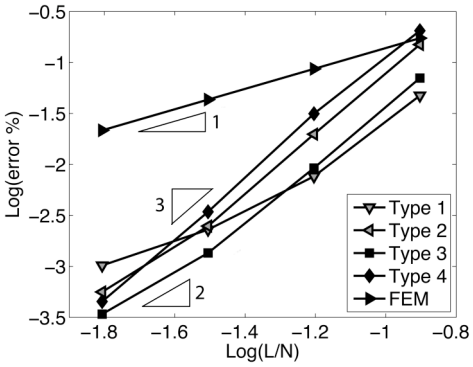

(a)

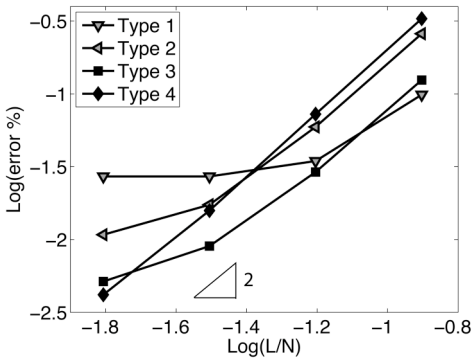

(b)

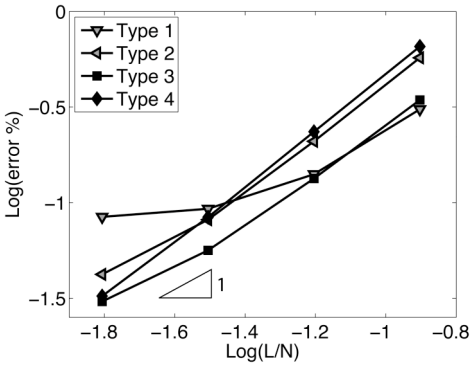

(c)

Fig 4.11 – Global convergence of stresses (a), first derivatives (b), second derivatives (c).

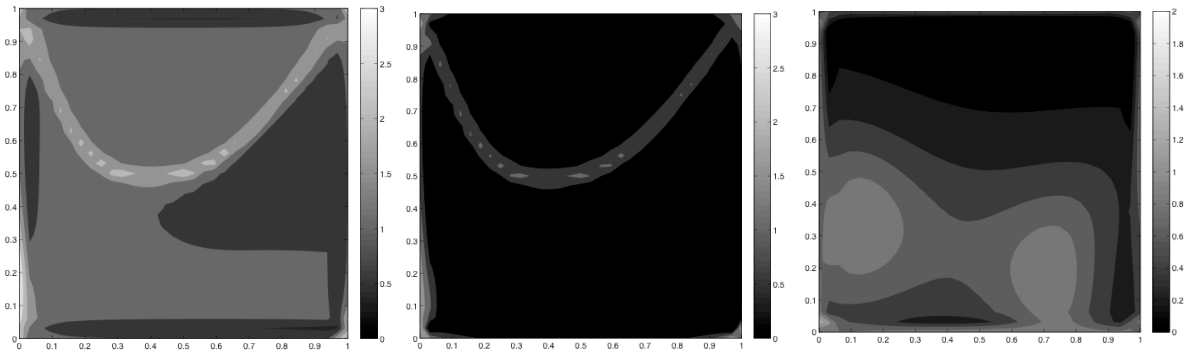

(a) (b) (c)

Fig 4.12 – Convergence maps of RCP Type 4. Stresses (a), First derivatives (b), Second derivatives (c)

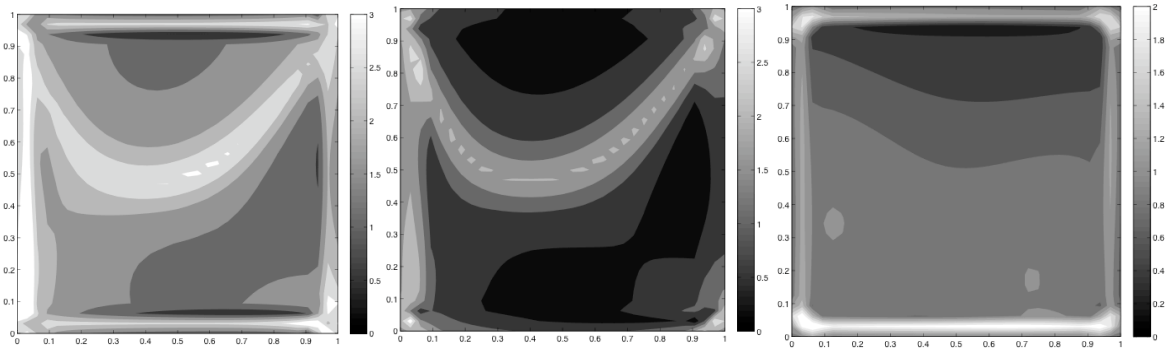

(a) (b) (c)

Fig 4.13 – Convergence maps of RCP Type 2. Stresses (a), First derivatives (b), Second derivatives (c)

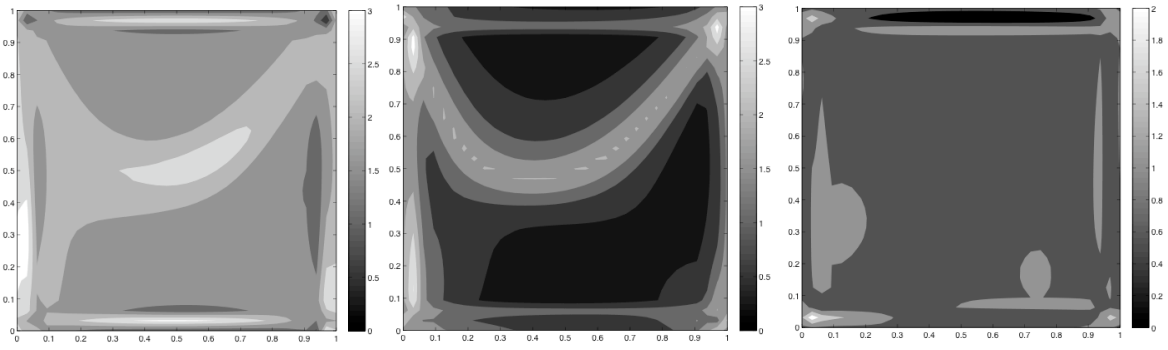

(a) (b) (c)

Fig 4.14 – Convergence maps of RCP Type 3. Stresses (a), First derivatives (b), Second derivatives (c)

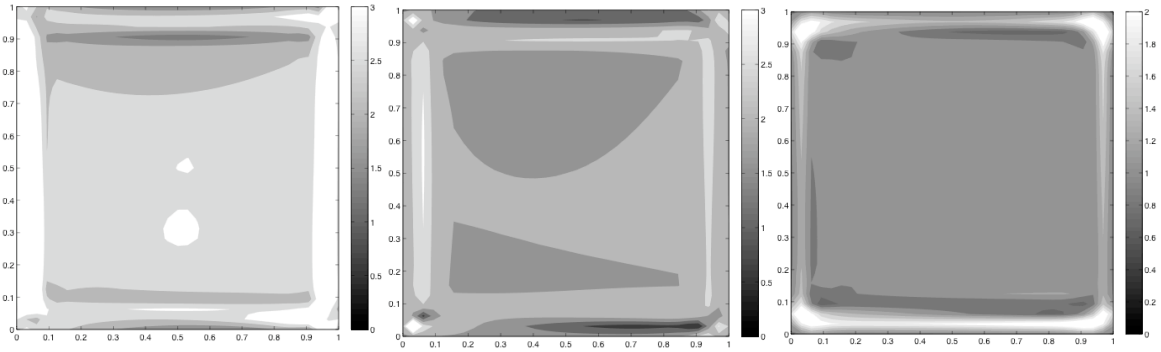

(a) (b) (c)

Fig 4.15 – Convergence maps of RCP Type 4. Stresses (a), First derivatives (b), Second derivatives (c)

For this test, a comparison between stresses accuracy reached with FEM, RCP Type 1 and RCP Type 4 is presented confirming the good performance of FEM at optimal stress points. Considering RCP it can be noticed that accuracy decrees moving from the centre to the border of the patch but in a much smoother way than FEM. These maps exclude that an effective improvement of the stress extraction procedure could be obtained averaging values coming from patches far from the point of interest like the ones enclosed in the second ring of patch type B. These results have been confirmed in numerical tests, that are not here reported, where stresses were extracted averaging information coming from all patches containing the point of interest.

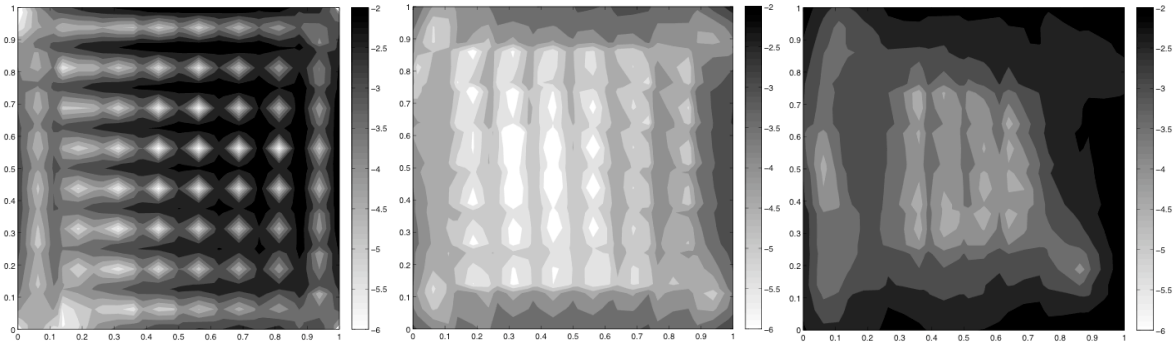

(a) (b) (c)

Fig 4.16 – Accuracy maps for 8x8 elements mesh. FEM (a), RCP Type 1 (b), RCP Type 4 (c)

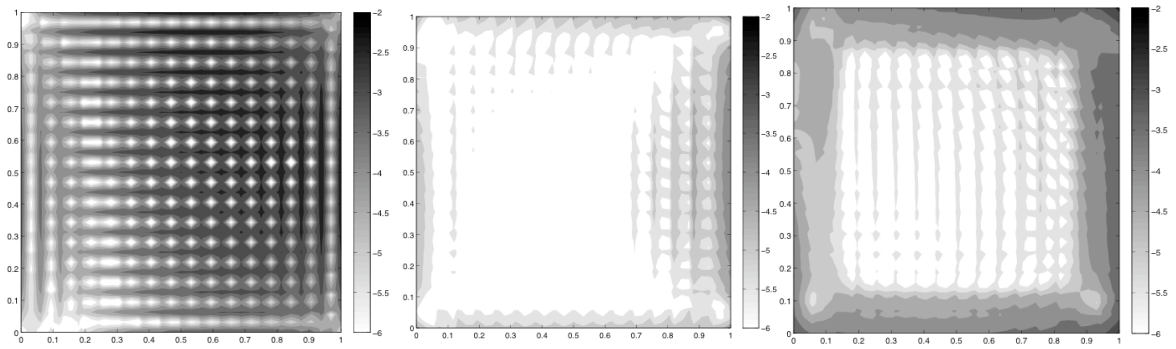

(a) (b) (c)

Fig 4.14 – Accuracy maps for 16x16 elements mesh. FEM (a), RCP Type 1 (b), RCP Type 4 (c)

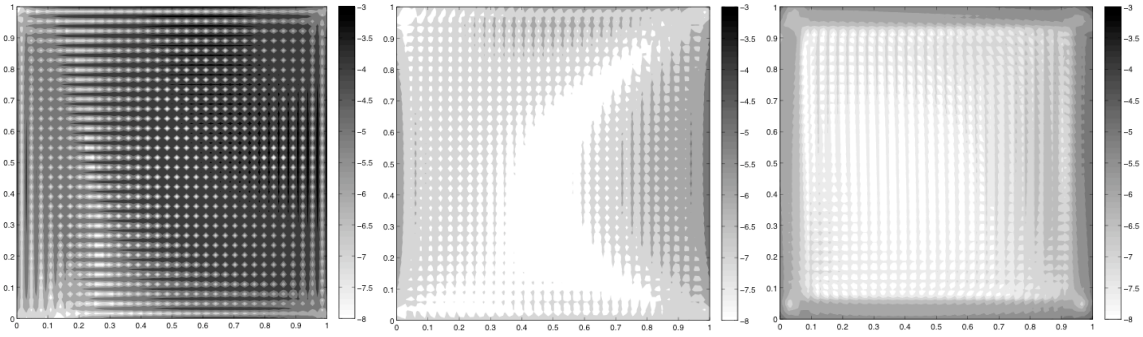

(a) (b) (c)

Fig 4.14 – Accuracy maps for 32 elements per side mesh. FEM (a), RCP Type 1 (b), RCP Type 4 (c)

From the presented data it can be concluded that RCP Type 1 is the most suitable if recovery is performed in order to drive mesh refinement, as its accuracy is always better that FEM in every point of the domain. RCP Type 3 and Type 4 are the most suitable if stable convergence of stress derivatives is needed like in transverse stress profiles reconstruction in laminated plates (Chapter 9).

Chapter 4

RCP-based recovery on derivatives

This recovery technique can be considered a mixed form between the *Double L^2 -projection* described in [4] and RCP as it substantially add equilibrium constraint to the first one using RCP procedure even though, in this case, the minimization has not precise physical meaning.

In fact, it can be easily observed that if a matrix of self-equilibrated modes is derived with respect of one axis direction, the resultant matrix of derivative modes is equivalent to a matrix of self-equilibrated modes with one less degree of completeness.

For example, consider the matrix of quadratic self-equilibrated modes for membrane stress resultants that appears in the reconstructed solution (2.1), analogous to (2.5):

$$\begin{bmatrix} N_x^r \\ N_y^r \\ N_{xy}^r \end{bmatrix} = \begin{bmatrix} 1 & 0 & 0 & y & 0 & x & 0 & y^2 & 0 & x^2 & 2xy & 0 \\ 0 & 1 & 0 & 0 & x & 0 & y & 0 & x^2 & y^2 & 0 & 2xy \\ 0 & 0 & 1 & 0 & 0 & -y & -x & 0 & 0 & -2xy & -y^2 & -x^2 \end{bmatrix} \alpha + \begin{bmatrix} N_x^p \\ N_y^p \\ N_{xy}^p \end{bmatrix} \quad (4.1)$$

If the derivatives with respect of the x axis of the (4.1) are considered:

$$\begin{bmatrix} d_x N_x^r \\ d_x N_y^r \\ d_x N_{xy}^r \end{bmatrix} = \begin{bmatrix} 0 & 0 & 0 & 0 & 0 & 1 & 0 & 0 & 0 & 2x & 2y & 0 \\ 0 & 0 & 0 & 0 & 1 & 0 & 0 & 0 & 2x & 0 & 0 & 2y \\ 0 & 0 & 0 & 0 & 0 & 0 & -1 & 0 & 0 & -2y & 0 & -2x \end{bmatrix} \boldsymbol{\alpha} + \begin{bmatrix} d_x N_x^p \\ d_x N_y^p \\ d_x N_{xy}^p \end{bmatrix} \tag{4.2}$$

It can be noticed that the matrix that appear in the new equation (4.2) is still a matrix of self-equilibrated modes but with one less degree of completeness.

If two RCP procedure are performed introducing derivatives of stress resultants with respect to one axis each time instead of stress resultants, identity matrix is introduced instead of inverse of constitutive matrix and the derivative of the particular solution with respect to the considered axis is introduced instead of the particular solution, the procedure is transformed in a L^2-projection of derivatives among a set of derivatives modes descending from a set of self-equilibrated stress modes.

$$\int_{\Omega_p} \left[\delta dN^{rT} \left(dN^r - dN^h \right) + \delta dM^{rT} \left(dM^r - dM^h \right) + \delta dS^{rT} \left(dS^r - dS^h \right) \right] d\Omega_p$$

$$\forall \left(\delta dN^r, \delta dM^r, \delta dS^r \right) \tag{4.3}$$

where Ω_p is the patch domain, $\left(dN^r, dM^r, dS^r \right)$ are the recovered stresses derivatives with respect of one axis and $\left(dN^h, dM^h, dS^h \right)$ are the stresses derivatives with respect of the some axis resulting from the fist RCP or FEM solution if high order elements are used.

Two different values for the mixed second order derivatives are obtained from this procedure so that averaging between them is needed.

No results are shown for this procedure as, at this stage, does not seem competitive with other procedures here presented but it might be investigated if higher order derivatives are needed.

Chapter 5

Last Square Displacements (LSD)

The idea of Last Square Displacements (LSD) steams from a very simple observation: if we extract stresses using the traditional method introducing exact nodal displacements instead of values coming from Finite Element analysis, no improvement in accuracy or convergence rate of stress resultants is observed (Fig 5.1).

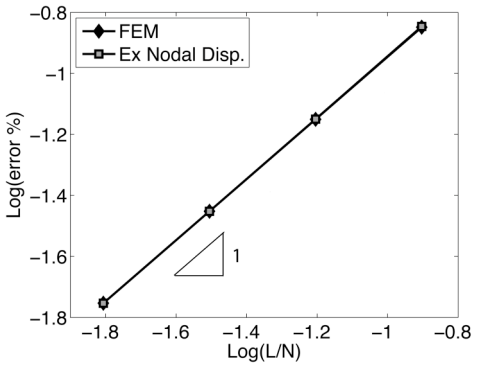

Fig 5.1 – Global convergence rate for Fem and Fem using exact nodal values for Problem 2.

This means that the preponderant contribution to error affecting stress resultants is not introduced in the global resolution, when nodal displacements are calculated, but in the subsequent step when strains are obtained deriving shape functions.

Moving from this observation a new recovery technique has been developed aimed at preserving information since the beginning, that is to say, avoiding shape function derivation in order to obtain strains and than stress resultants via constitutive matrix.

Many different implementations of this idea can be developed but the simplest one is to use a patch-based approach where displacements nodal values are interpolated using a last square scheme over the patches leading to continuous displacement fields in the patch domain.

Each displacement component is interpolated separately and its derivatives are calculated directly in every point of interest. Element-patch and node-patch based approaches are possible exactly like in RCP (see Chapter 2) but here only the first one is presented as it does not require any additional averaging after last square minimization and for this reason can be considered the most cost effective between the two possibilities.

In this case it is crucial to extend border patches with the procedure presented for RCP so that patches will contain at least a minimum number of nodes ensuring that the pseudoinverse matrix is not singular.

Here, in order to estimate second order derivatives of stress resultants a complete set of cubic polynomials have been chosen to reconstruct each displacement field from nodal values so that estimation for second order derivatives of stresses (that is to say third order derivatives of displacements) is obtained.

For each displacement field a new representation is introduced:

$$u_i^r(x,y) = \begin{bmatrix} 1 & x & y & xy & x^2 & y^2 & x^2y & y^2x & x^3 & y^3 \end{bmatrix} [\alpha] \tag{5.1}$$

where $u_i^r(x,y)$ is the recovered field for the *i-th* displacement component and α is a vector of unknown parameters. Patch reference system is based on the centre of the element the patch refers to, like in RCP procedure.

If u_{ij} is the value of the *i-th* displacement component in the *j-th* node of the current patch and x_j, y_j are the *j-th* node values of the local coordinates then for each node over the patch we can write:

$$\begin{bmatrix} u_i^r(x_{j-1},y_{j-1}) \\ u_i^r(x_j,y_j) \\ u_i^r(x_{j+1},y_{j+1}) \end{bmatrix} = \begin{bmatrix} 1 & x_{j-1} & y_{j-1} & x_{j-1}y_{j-1} & x_{j-1}^2 & y_{j-1}^2 & x_{j-1}^2 y & y_{j-1}^2 x & x_{j-1}^3 & y_{j-1}^3 \\ 1 & x_j & y_j & xy_j & x_j^2 & y_j^2 & x_j^2 y_j & y_j^2 x_j & x_j^3 & y_j^3 \\ 1 & x_{j+1} & y_{j+1} & x_{j+1}y_{j+1} & x_{j+1}^2 & y_{j+1}^2 & x_{j+1}^2 y_{j+1} & y_{j+1}^2 x & x_{j+1}^3 & y_{j+1}^3 \end{bmatrix} [\alpha] \tag{5.2}$$

that, using other symbols, can be written as:

$$\boldsymbol{u}_i = \boldsymbol{A}\boldsymbol{\alpha} \tag{5.3}$$

than OLS minimization leads to:

$$\boldsymbol{\alpha} = \left(\boldsymbol{A}^T\boldsymbol{A}\right)^{-1}\boldsymbol{A}^T\boldsymbol{u}_i \tag{5.4}$$

that can be solved providing unknown parameters $\boldsymbol{\alpha}$.

Once vector $\boldsymbol{\alpha}$ has been estimated the reconstructed displacement field is known point wise in the patch domain as well as its derivatives that physically represent strains and strains derivatives. Thus, using constitutive equations, stress resultants and their derivatives can be obtained.

The procedure is simple and cost effective, as it requires in input only data directly available after Finite Element solution without any additional post processing in order to evaluate stress resultants in the traditional way and can be easily extended to three-dimensional problems and to other physical fields in order to use low order elements ensuring convergence of first, second and third derivatives of the principal variable.

At the present stage the procedure has been tested only in regular meshes but the extreme robustness of the OLS method has been widely verified for example in Quadratic Fitting (QF) method used in [4].

Moreover, numerical tests indicate that LSD is an ultraconvergent procedure as it is able to exactly recover the analytical solution for cubic displacements fields when linear shape functions are used in the finite element analysis.

Chapter 6

Numerical tests for LSD

For these tests patch Type A has been used as it has shown to provide best performances with the minimum computational cost. In general, as already observed for RCP, using larger patches ensure higher convergence rate but decrees accuracy for coarse meshes.

Problem 1

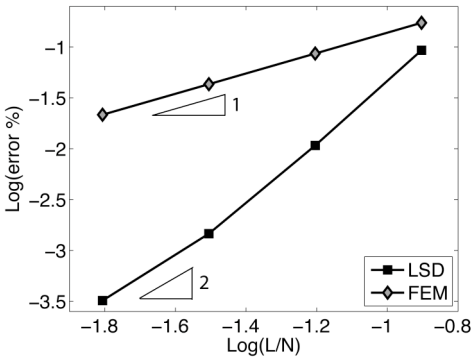

(a)

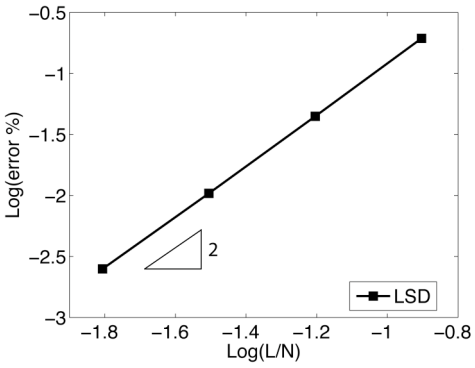

(b)

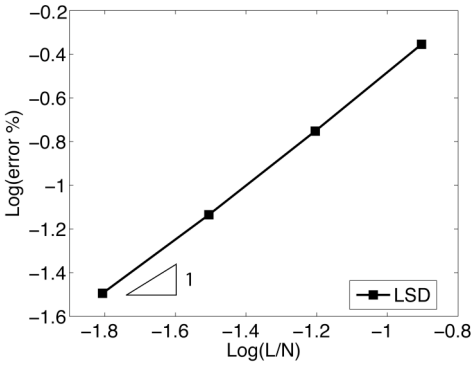

(c)

Fig 6.1 – Convergence of stresses (a), first derivatives (b) and second derivatives (c)

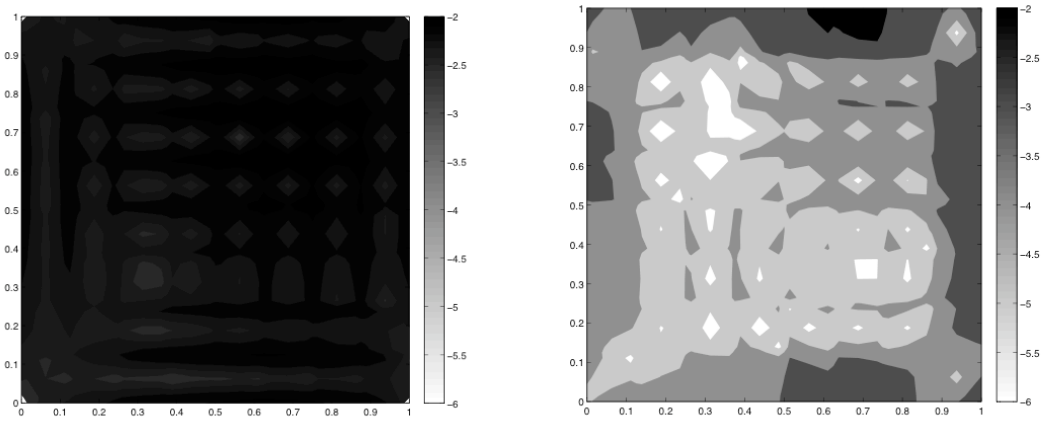

(a) (b)

Fig 6.2 – Accuracy maps for 8 elements per side mesh. FEM (a), LSD (c)

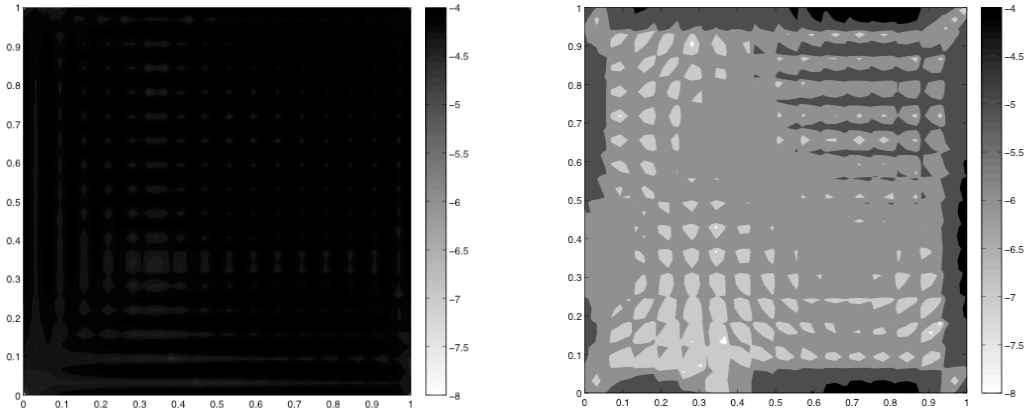

(a) (b)

Fig 6.3 – Accuracy maps for 16 elements per side mesh. FEM (a), LSD (c)

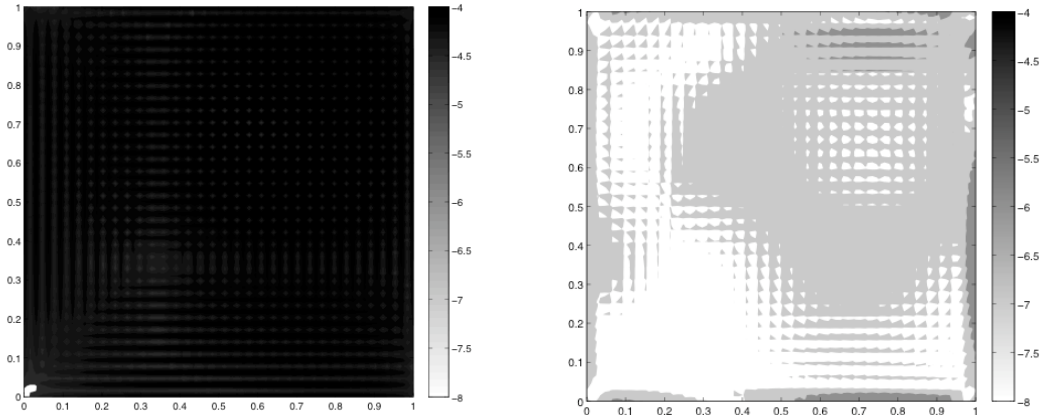

(a) (b)

Fig 6.4 – Accuracy maps for 32 elements per side mesh. FEM (a), LSD (c)

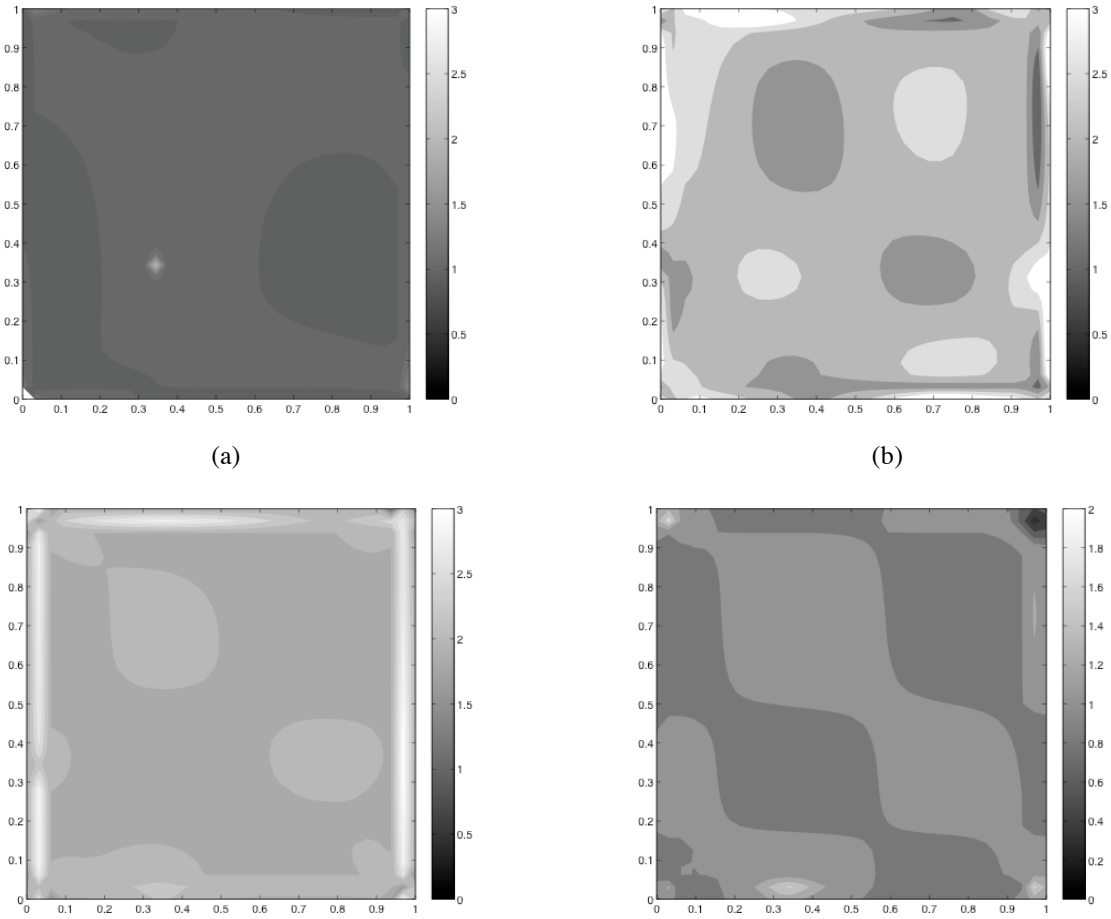

(a) (b)

(c) (d)

Fig 6.5 – Convergence maps. Fem stresses (a), LSD stresses (b), LSD first derivatives (c), LSD second derivatives (d)

Problem 2

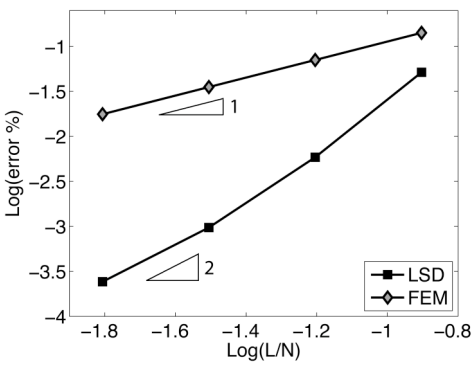

(a)

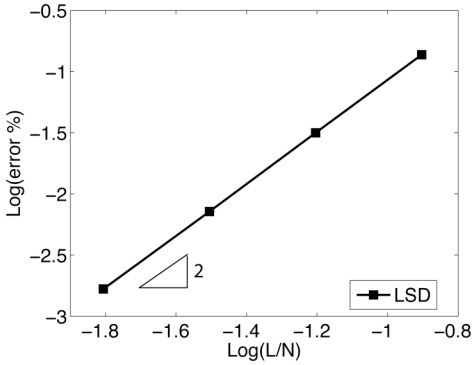

(b)

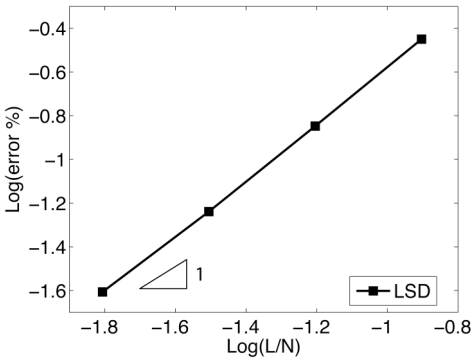

(c)

Fig 6.6 – Convergence of stresses (a), first derivatives (b) and second derivatives (c)

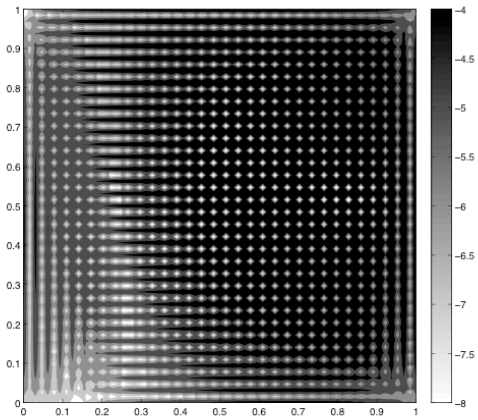

(a)

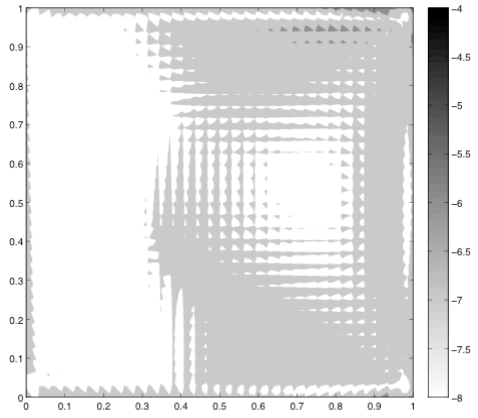

(b)

Fig 6.7 – Accuracy maps for 32 elements per side mesh. FEM (a), LSD (b)

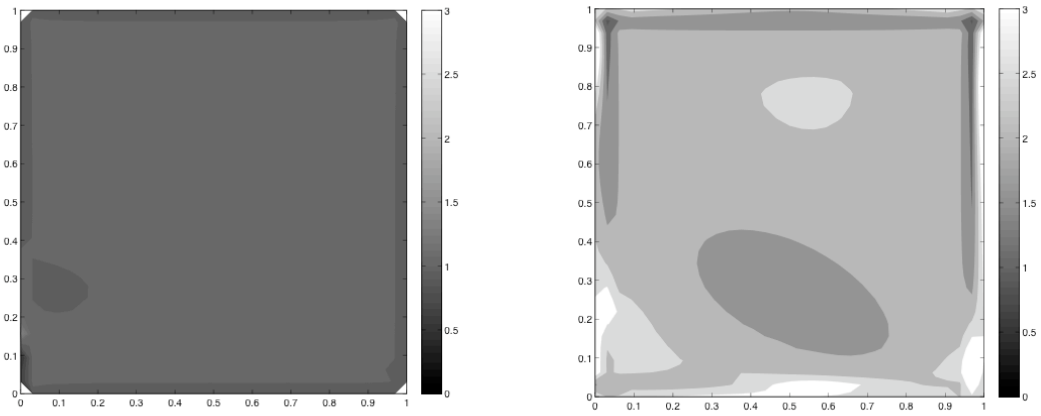

(a) (b)

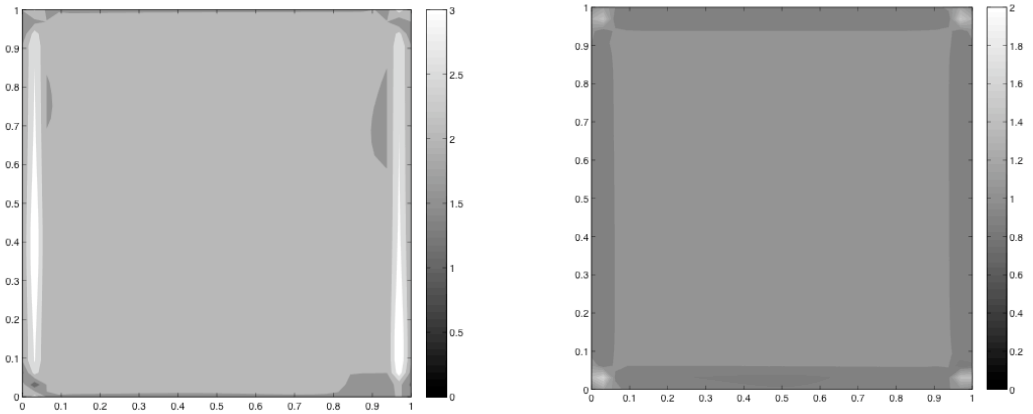

(c) (d)

Fig 6.8 – Convergence maps. Fem stresses (a), LSD stresses (b),

LSD first derivatives (c), LSD second derivatives (d)

Problem 3

Problem 3 is here used to prove ultraconvergence of the procedure. Other tests, using cubic displacement fields, clearly confirmed this result.

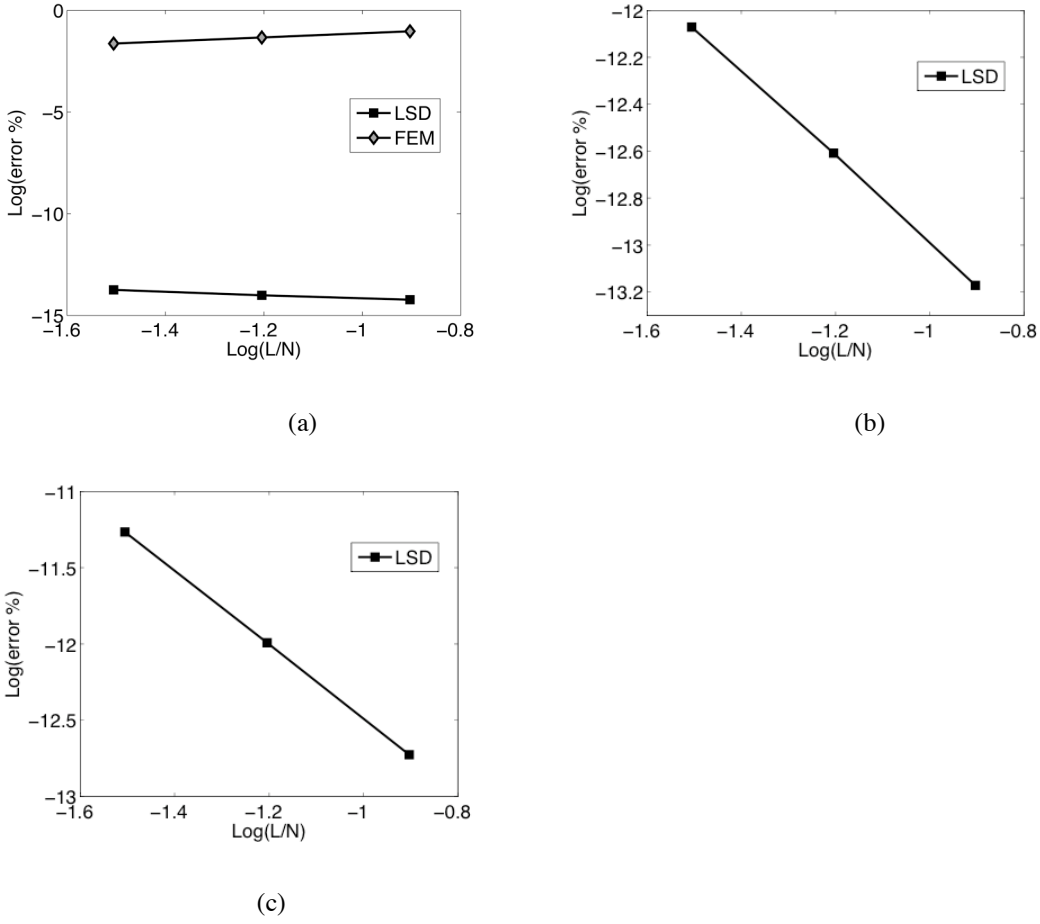

Fig 6.9 – Convergence of stresses (a), first derivatives (b) and second derivatives (c)

Great accuracy confirms that exact solution has been recovered but error associated to first and second stress derivatives rapidly increases with mesh refinements. The same behaviour was observed in [4] using the so-called Quadratic Fitting (QF). In that case it has been explained thinking that the function to recover becomes nearly constant if fine meshes are used and derivation becomes sensitive to numerical errors.

Chapter 7

Transverse stress profiles reconstruction for laminated plates

Composite laminated plates are nowadays widely used in many different structural applications and a number of laminate theories have been proposed in literature [8]. Among these, the First-order Shear Deformation Theory (FSDT) is usually considered a good compromise between accuracy and computational efficiency. However, it must be noted that in FSDT transverse shear deformation effects are accounted for in a simplified manner while transverse normal effects are completely neglected.

A hybrid-stress finite element for the analysis of FSDT composite laminated plates and an effective procedure to reconstruct transverse shear stresses profiles have been recently proposed in [5]. There, to guarantee convergence of the reconstruction strategy, stress resultants entering the reconstruction process are first recovered using RCP.

Here, the same finite element formulation is used [5] and attention is focused on reconstruction of transverse normal stress profiles. Once accurate transverse shear stresses are reconstructed, three-dimensional force equilibrium in the thickness direction is used to compute the transverse normal stress profile. Indeed, the accuracy of this reconstruction depends on the accuracy of second derivatives of stress resultants. In fact three dimensional undefined equilibrium conditions can be written as:

$$\boldsymbol{D}_p^* \boldsymbol{s} - \nabla_z \boldsymbol{\tau} - \boldsymbol{b}_x = 0 \,, \quad \boldsymbol{D}_s^* \boldsymbol{\tau} - \nabla_z \sigma_z - b_z = 0 \tag{7.1}$$

where $\boldsymbol{b}_x$ is the vector of in-plane body forces, b_z is the transverse body force and ∇_z the derivative with respect to z. The only unknowns, once stress resultants derivatives are identified, are $\boldsymbol{\tau}$ and $\boldsymbol{\sigma}_z$. Integrating these equations in the thickness direction, imposing boundary conditions on top and bottom faces of the laminate, interlaminar continuity and the static equivalence with shear transverse stress resultants $\boldsymbol{S}$, transverse stress profiles can be reconstructed.

Introducing for convenience inverse relations for (1.9):

$$\boldsymbol{\mu} = \boldsymbol{F}_m \boldsymbol{N} + \boldsymbol{F}_{mb} \boldsymbol{M} \qquad \boldsymbol{\chi} = \boldsymbol{F}_{mb} \boldsymbol{N} + \boldsymbol{F}_b \boldsymbol{M} \qquad \boldsymbol{\gamma} = \boldsymbol{F}_s \boldsymbol{S} \tag{7.2}$$

Resulting equations for transverse shear stresses are:

$$\boldsymbol{\tau}(z) = -\boldsymbol{p}_x^{(-)} + \int_{-h/2}^{z} \left(\boldsymbol{D}_p^* \boldsymbol{s} - \boldsymbol{b}_x \right) dz\,, \tag{7.3}$$

where in-plane stresses $\boldsymbol{s}$ are obtained from the solution of the plate problem:

$$\boldsymbol{s} = \boldsymbol{C}_m^{(k)} \left[\left(\boldsymbol{F}_m \boldsymbol{N} + \boldsymbol{F}_{mb} \boldsymbol{M} \right) + z \left(\boldsymbol{F}_{mb} \boldsymbol{N} + \boldsymbol{F}_b \boldsymbol{M} \right) \right] \tag{7.4}$$

and transverse normal stress profile is reconstructed as:

$$\sigma(z) = -p_z^{(-)} + \int_{-h/2}^{z} \left(\boldsymbol{D}_s^* \boldsymbol{\tau}(z) - b_z \right) dz \tag{7.5}$$

being $\boldsymbol{p}_x^{(-)}$ and $p_z^{(-)}$ the in surface traction on the laminate bottom face.

It can be proved that, if $\boldsymbol{N}$, $\boldsymbol{M}$ and $\boldsymbol{S}$ satisfy equilibrium condition (1.7), the reconstructed stress profile automatically meet all reported conditions.

This means that, if RCP is used to recover stress resultants and calculate their derivatives, the transverse profiles reconstruction procedure is extremely simple and there is no need of corrections to meet the boundary condition at the top of the laminate once the bottom one is imposed.

Chapter 8

8.1 Transverse stress profiles reconstruction: numerical results

A simply supported square laminated plate is considered under sinusoidal load of unit maximum intensity. Side length L and thickness h are chosen equal respectively to *9* and *0.9* so that L/h ratio is *10*. Thanks to the double in-plane symmetry only a quarter of the plate is considered.

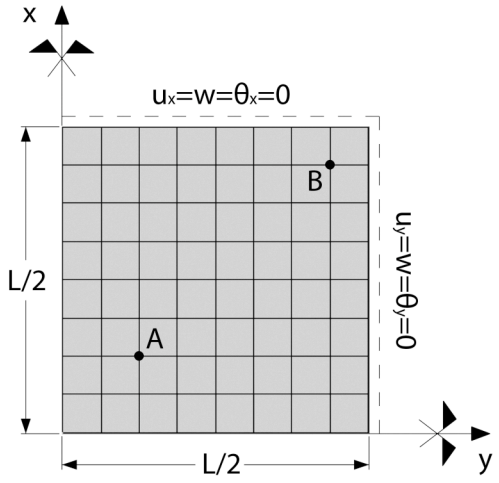

Fig. 8.1 – Simply supported square plate with 8x8 mesh.

Two staking sequences are considered: a symmetric (0/90/0) and an antisymmetryc (0/90). Lamina mechanical properties are:

$$E_b = 10^5\,, \qquad E_a = 25E_b\,, \qquad \nu_{ab} = 0.25\,, \qquad G_{ac} = G_{ab} = 0.5E_b\,, \qquad G_{bc} = 0.2E_b$$

Shear correction factors for cylindrical bending are assumed as proposed in [9] and are considered as constant values. Even though here is not presented, an iterative procedure could be implemented in order to update shear correction factors to the value descending from the reconstructed shear stress profiles.

In this case constant values are chosen as $k_{11} = 235445 / 404004$, $k_{22} = 289 / 360$, $k_{12} = 0$ for (0/90/0) and $k_{11} = k_{22} = 297680 / 362481$, $k_{12} = 0$ for (0/90). Reference solutions have been calculated according to [8].

Seemingly to plain stress cases presented in previous chapters, error convergence graphs and maps are obtained in order to validate the effectiveness of the procedures.

Differently from plane cases, here, the degree of completeness of polynomial expansion is not the some for all stress resultants when RCP is used. In fact, if self-equilibrated modes are considered, shear resultants can be obtained as a linear combination of moments first derivatives so that they necessarily have one less degree of completeness. This means that, in the matrix of self-equilibrated modes, they are accounted for in a more simplified way.

For example, consider the matrix of self-equilibrated modes if a complete quadratic representation is chosen for the reconstruction of moments and shear resultants (2.1):

$$\begin{bmatrix} M_x^r \\ M_y^r \\ M_{xy}^r \\ S_x^r \\ S_y^r \end{bmatrix} = \begin{bmatrix} 1 & 0 & 0 & x & y & 0 & 0 & 0 & 0 & xy & 0 & x^2 & y^2 & 0 & 0 & 0 & 0 \\ 0 & 1 & 0 & 0 & 0 & x & y & 0 & 0 & 0 & xy & 0 & 0 & x^2 & y^2 & 0 & 0 \\ 0 & 0 & 1 & 0 & 0 & 0 & 0 & x & y & 0 & 0 & -xy & 0 & 0 & -xy & x^2 & y^2 \\ 0 & 0 & 0 & 1 & 0 & 0 & 0 & 0 & 1 & y & 0 & x & 0 & 0 & -x & 0 & 2y \\ 0 & 0 & 0 & 0 & 0 & 0 & 1 & 1 & 0 & 0 & x & -y & 0 & 0 & y & 2x & 0 \end{bmatrix} \boldsymbol{\alpha} + \begin{bmatrix} M_x^p \\ M_y^p \\ M_{xy}^p \\ S_x^p \\ S_y^p \end{bmatrix}$$

(8.1)

In order to respect equilibrium equations (1.7) shear resultants $\boldsymbol{S}$ can be at most linear.

Another crucial point is that RCP is based on minimization of complementary energy on patches. In this case, as the considered plate is thin, shear energy is very small compared to bending one so that recovery enhances moments with better results than shear resultants. However it must be noted that, if energy associated to shear would increase, for example considering a thick plate, the procedure would automatically account for that.

Nonetheless, it must be noted that, in order to perform the transverse stress profile reconstruction as described in Chapter 7, only in-plane stress resultant derivatives are required so that no concern arises if transverse shear stress resultants derivatives are not convergent.

Finally it must be noted that staking sequence (0/90) shows membrane-bending coupling so that membrane-bending total energy must be considered:

$$e_{mn} = \frac{1}{2}\begin{bmatrix} \boldsymbol{N} - \boldsymbol{N}_{ex} \\ \boldsymbol{M} - \boldsymbol{M}_{ex} \end{bmatrix}^T \begin{bmatrix} \boldsymbol{F}_m & \boldsymbol{F}_{mb} \\ \boldsymbol{F}_{mb} & \boldsymbol{F}_b \end{bmatrix} \begin{bmatrix} \boldsymbol{N} - \boldsymbol{N}_{ex} \\ \boldsymbol{M} - \boldsymbol{M}_{ex} \end{bmatrix} \tag{8.2}$$

while the energy associated to transverse shear resultants is :

$$e_s = \frac{1}{2}\left[\boldsymbol{S} - \boldsymbol{S}_{ex}\right]^T \boldsymbol{F}_s \left[\boldsymbol{S} - \boldsymbol{S}_{ex}\right] \tag{8.3}$$

Once in-plane and transverse stress profiles are reconstructed it is possible to evaluate the three-dimensional error energy associated to the profiles. This is possible integrating the error energy through the thickness and associating the obtained value to the projection of the considered fibre on the xy plane:

$$e(x,y) = \frac{1}{2}\int_{-h/2}^{h/2} \left[\boldsymbol{\sigma}(x,y,z) - \boldsymbol{\sigma}_{ex}(x,y,z)\right] \boldsymbol{C}^{-1} \left[\boldsymbol{\sigma}(x,y,z) - \boldsymbol{\sigma}_{ex}(x,y,z)\right] dz \tag{8.4}$$

where $\boldsymbol{\sigma}$ is a vector containing the reconstructed three dimensional stresses, $\boldsymbol{\sigma}_{ex}$ contains the exact three dimensional stresses and $\boldsymbol{C}^{-1}$ is the inverse of the three dimensional constitutive matrix.

In subsequent profiles convergence graphs and maps, (8.4) has been obtained both considering the global three-dimensional energy and isolating energy associated to in-plane stresses, transverse shear stresses and transverse normal stresses related to stress resultants, stress resultant first derivatives and second derivatives respectively.

It must be noted that finite element stress resultants in case of RCP are obtained from the hybrid element [5] and in LSD are obtained deriving displacements fields. This explains the widely different performance of fem solution in (0/90) in evaluating shear resultants.

8.2 Numerical tests for RCP

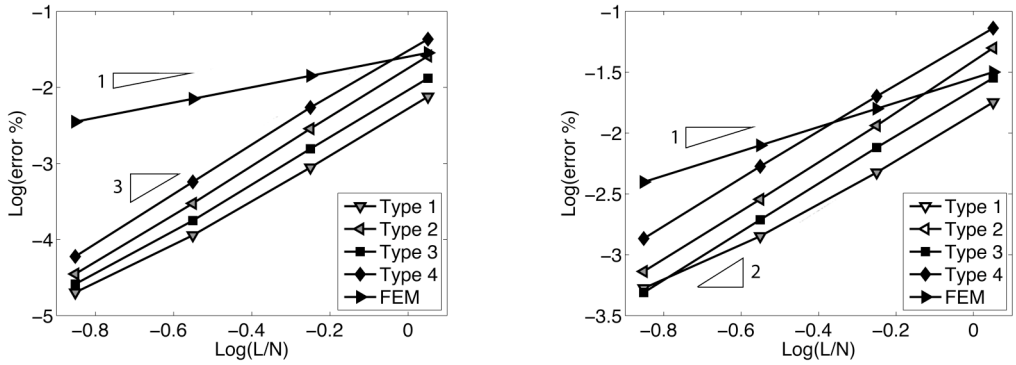

(a) (b)

Fig 8.2 – Global convergence of stress resultants for (0/90/0). Moments and membrane (a), Shear (b)

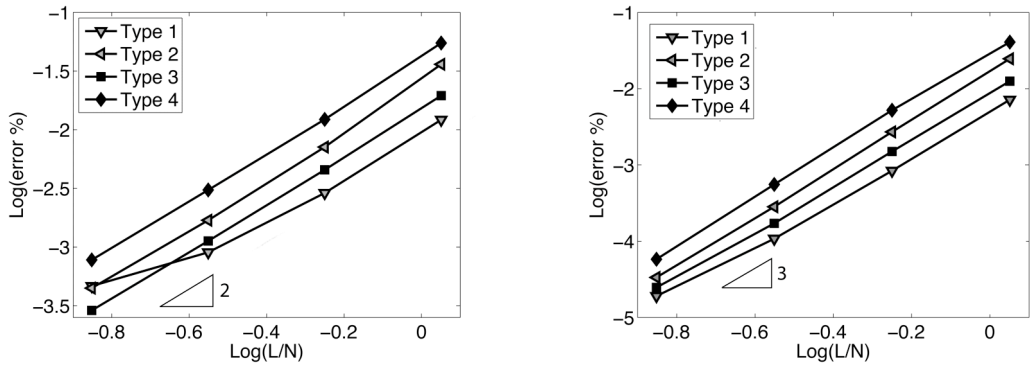

(a) (b)

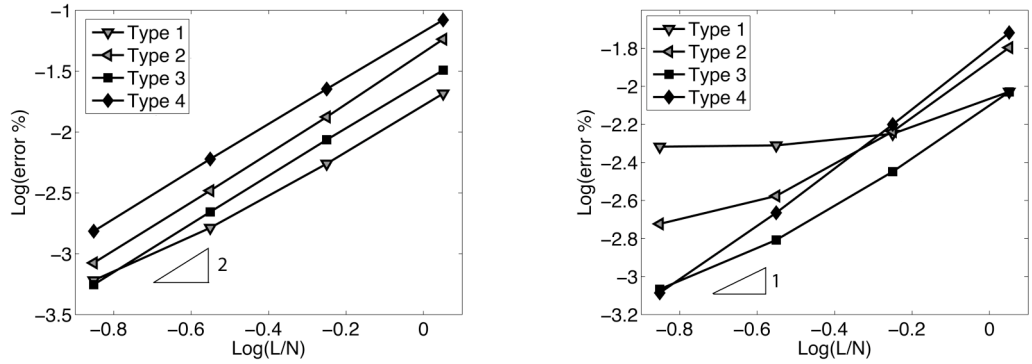

(c) (d)

Fig 8.3 – Global convergence of stress profiles in (0/90/0). Global energy (a), in-plane stresses (b), transverse shear stresses (c) transverse normal stresses (d).

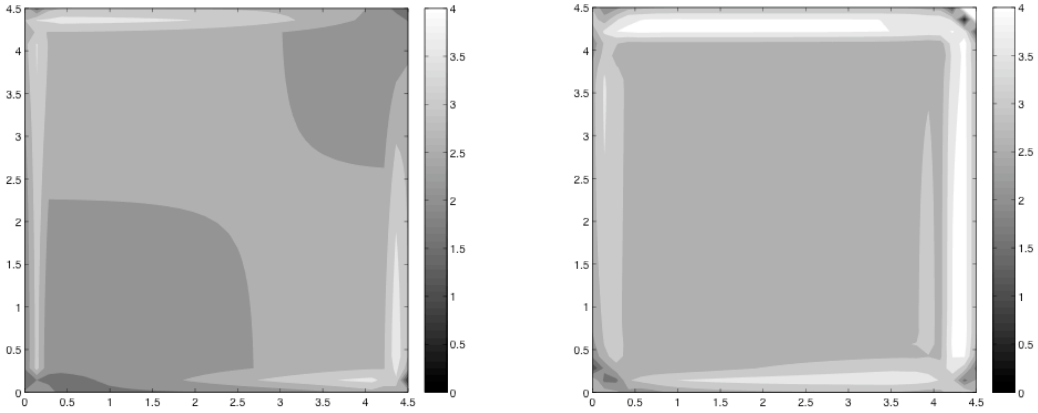

(a) (b)

Fig 8.4 – Convergence map for in plane stress profiles in (0/90/0). RCP Type 1 (a), RCP Type 4 (b)

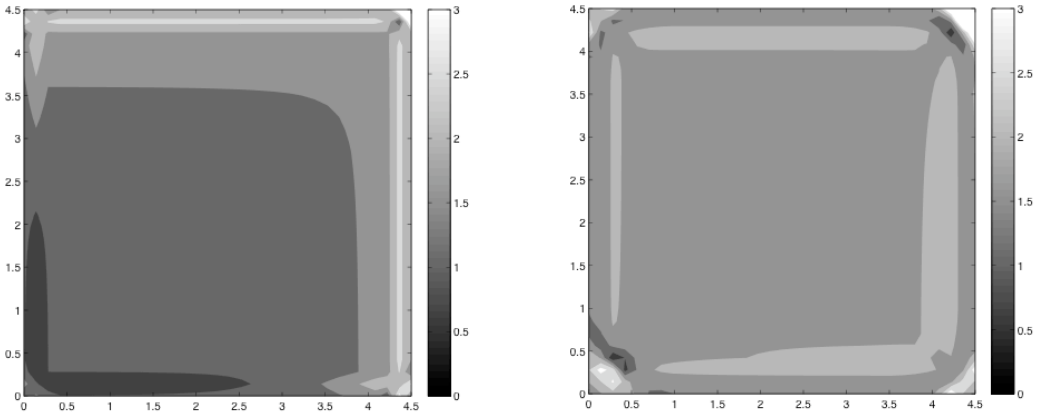

(a) (b)

Fig 8.5 – Convergence map for transverse shear stress profiles in (0/90/0). RCP Type 1 (a), RCP Type 4 (b)

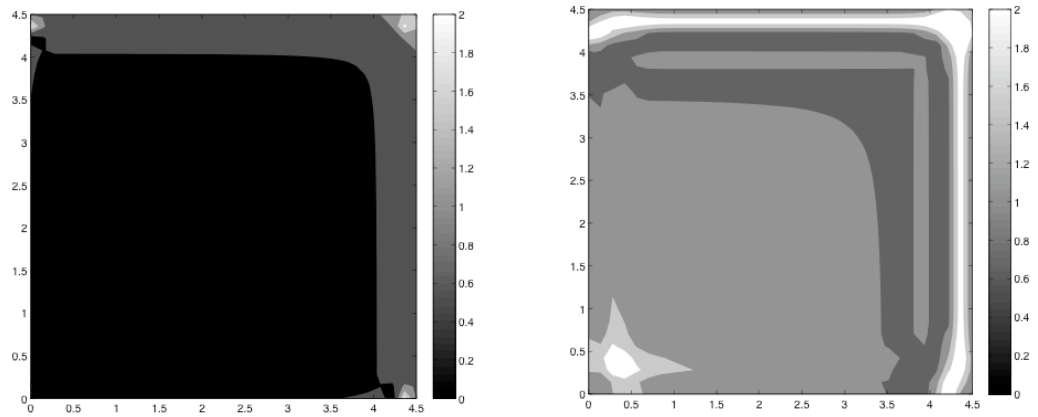

(a) (b)

Fig 8.6 – Convergence map for transverse normal stress profiles in (0/90/0). RCP Type 1 (a), RCP Type 4 (b)

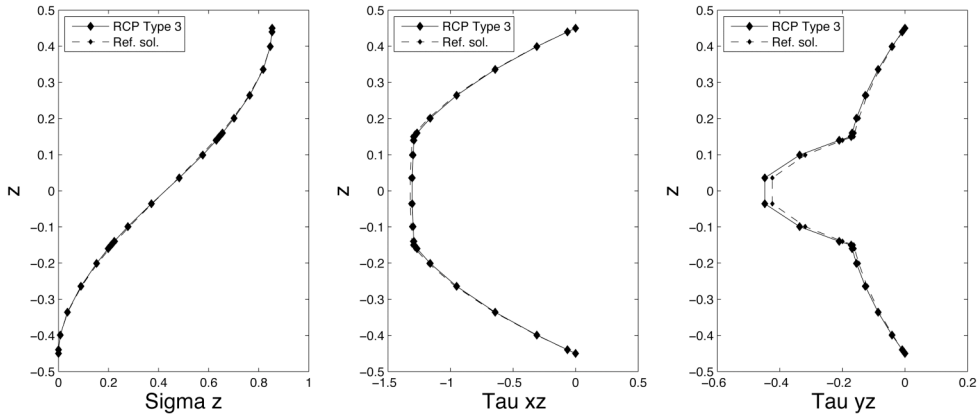

Fig 8.7 – Reconstructed transverse stress profiles at point A for (0/90/0) in an 8x8 mesh.

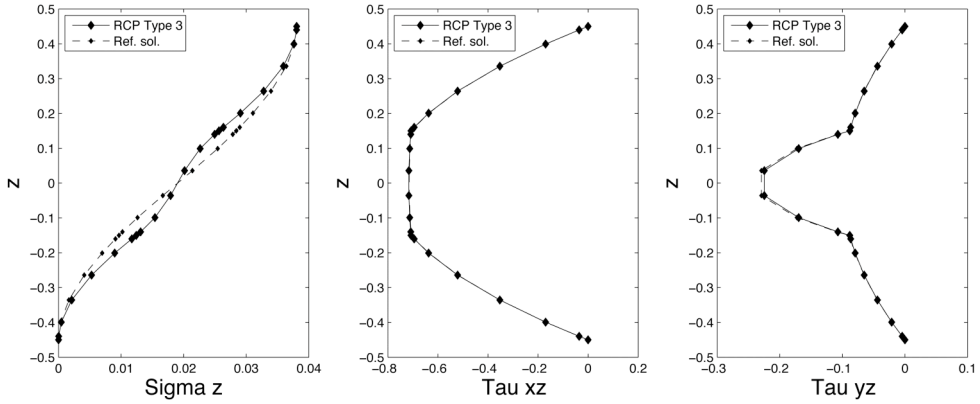

Fig 8.8 – Reconstructed transverse stress profiles at point B (0/90/0) in an 8x8 mesh.

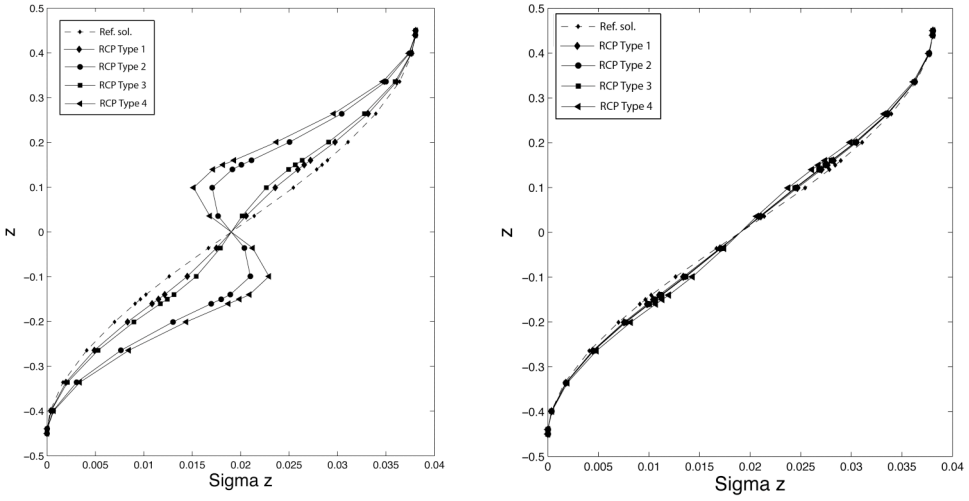

(a) (b)

Fig 8.9 – Reconstructed transverse normal stress profiles at point B (0/90/0). 8x8 mesh (a), 16x16 mesh (b).

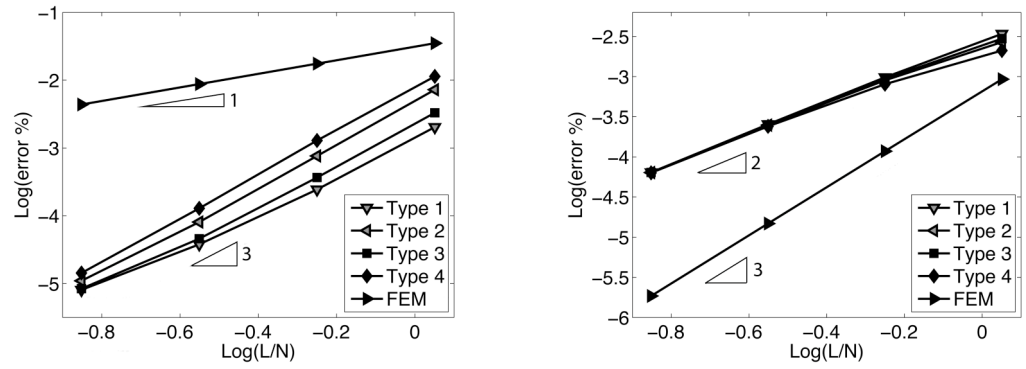

(a) (b)

Fig 8.7 – Global convergence of stress resultants for (0/90). Moments and membrane (a), Shear (b).

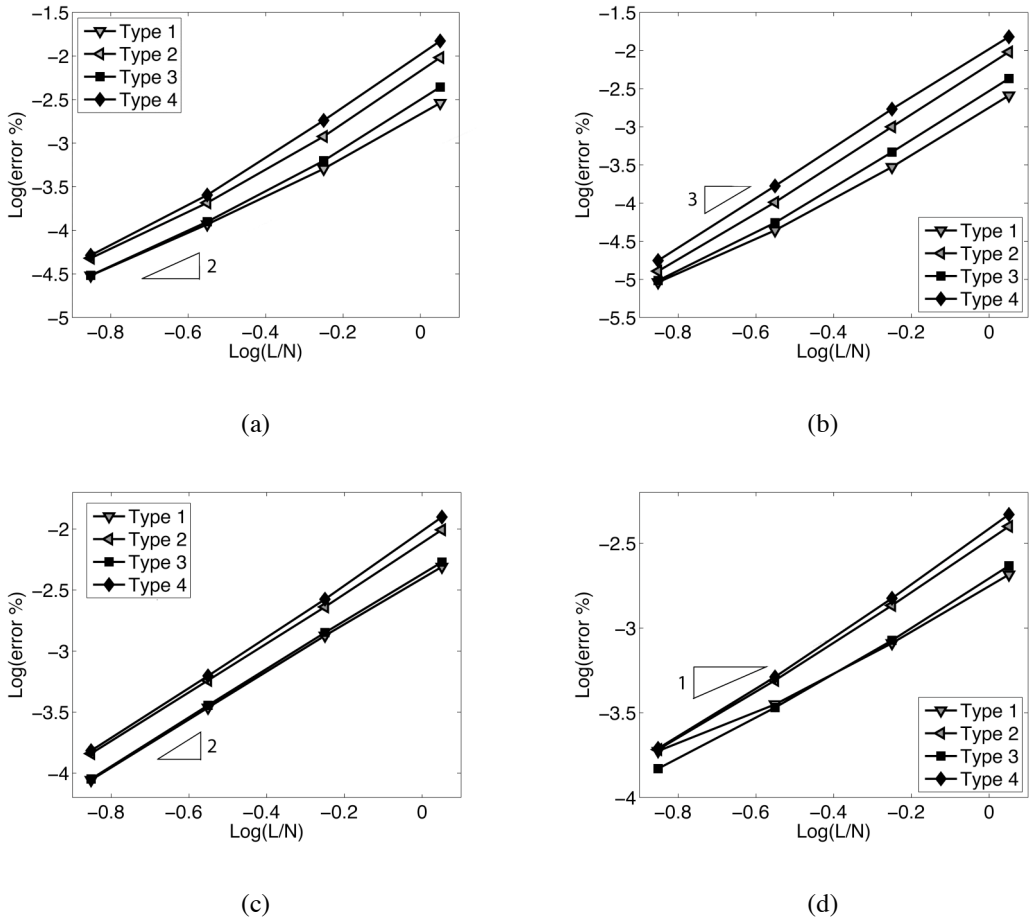

(a) (b)

(c) (d)

Fig 8.8 – Global convergence of stress profiles in (0/90). Global energy (a), In-plane stresses (b), transverse shear stresses (c) transverse normal stresses (d).

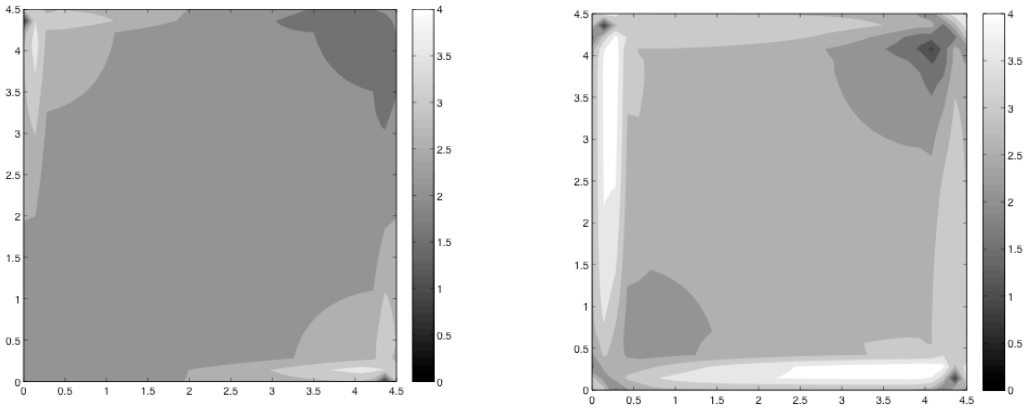

(a) (b)

Fig 8.9 – Convergence map for in plane stress profiles in (0/90). RCP Type 1 (a), RCP Type 4 (b)

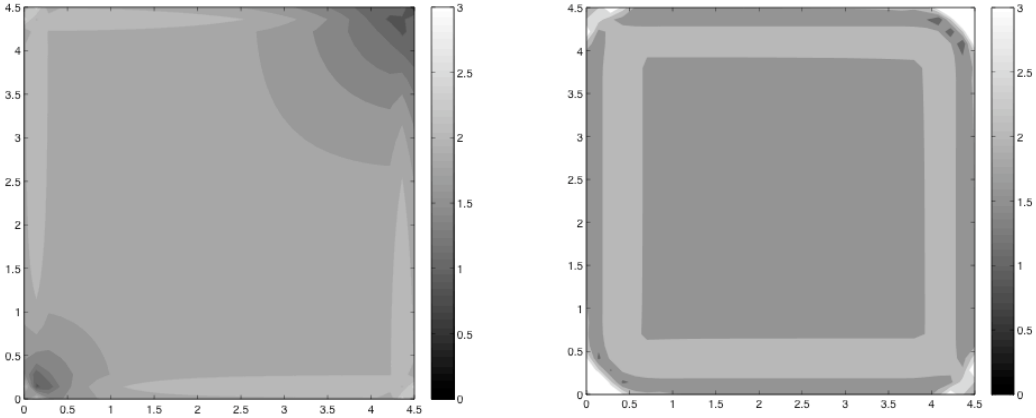

(a) (b)

Fig 8.10 – Convergence map for transverse shear stress profiles in (0/90). RCP Type 1 (a), RCP Type 4 (b)

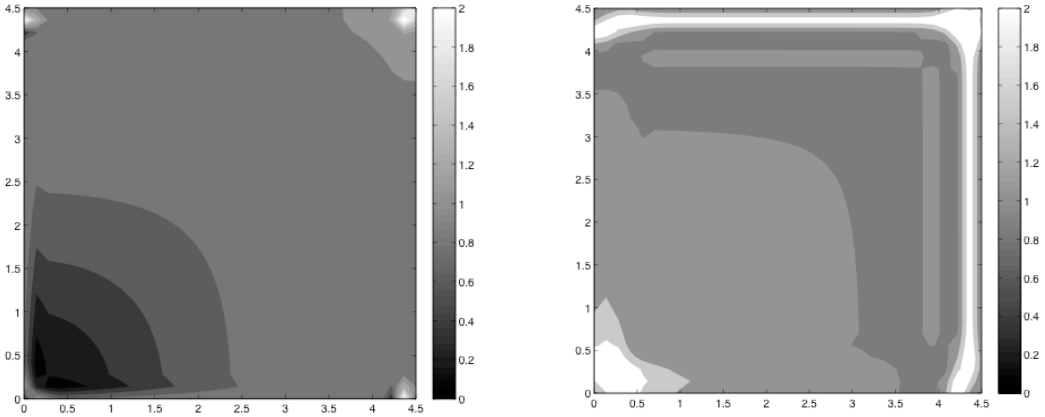

(a) (b)

Fig 8.11 – Convergence map for transverse normal stress profiles in (0/90). RCP Type 1 (a), RCP Type 4 (b)

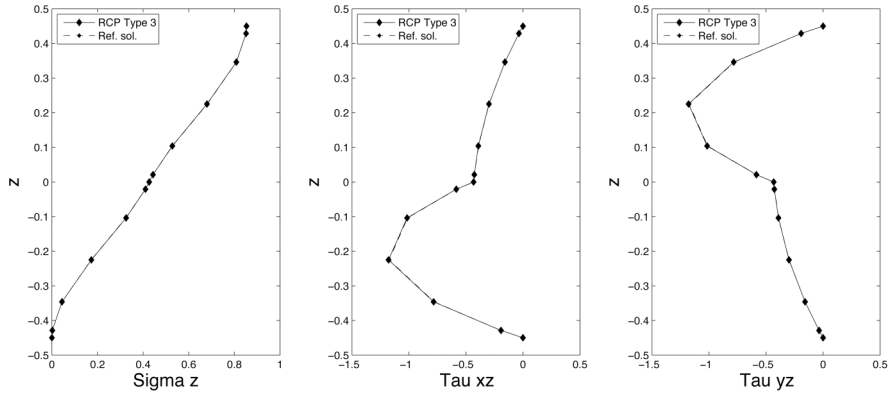

Fig 8.12 – Reconstructed transverse stress profiles at point A for (0/90/0) in an 8x8 mesh.

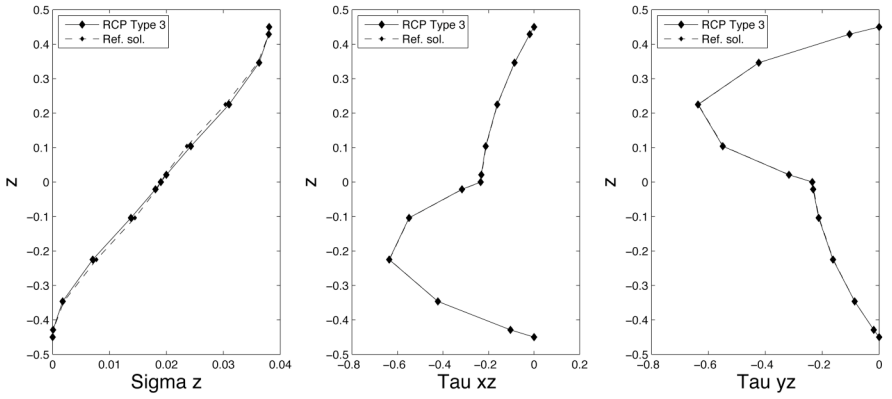

Fig 8.13 – Reconstructed transverse stress profiles at point A for (0/90/0) in an 8x8 mesh.

It can be clearly seen that RCP Type 3 ensure very accurate reconstructed profiles even if coarse meshes are used and that boundary conditions at the top and bottom side of the laminate are automatically satisfied if the proposed reconstruction procedure is used.

RCP Type 3 is the best combination between accuracy, convergence stability and computational cost. RCP Type 1 is very accurate and has a small computational cost but does not ensure convergence of the reconstructed transverse normal stress profiles.

Enlarging the patch, like in RCP Type 3 and 4, does not seem to be a convenient strategy as it leads to inaccurate second order derivatives and, thus, transverse normal stress profiles (especially at the domain border) although it ensures convergence of the reconstructed profiles everywhere in the domain.

8.3 Numerical tests for LSD

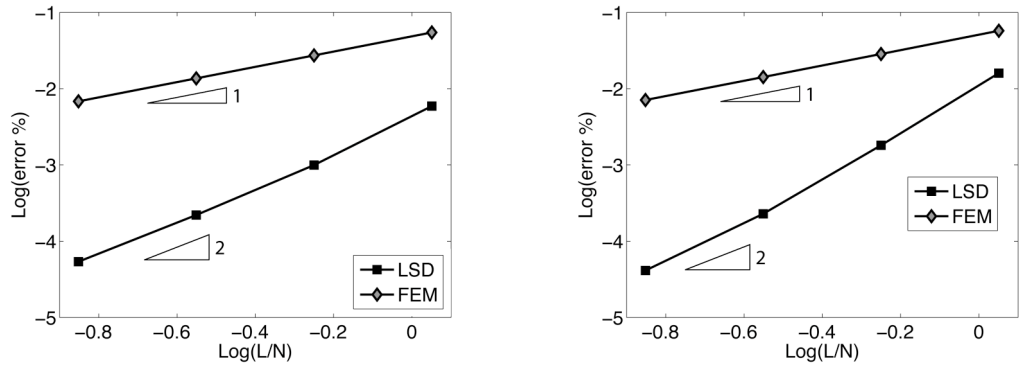

(a) (b)

Fig 8.14 – Global convergence of stress resultants for (0/90/0). Moments and membrane (a), Shear (b)

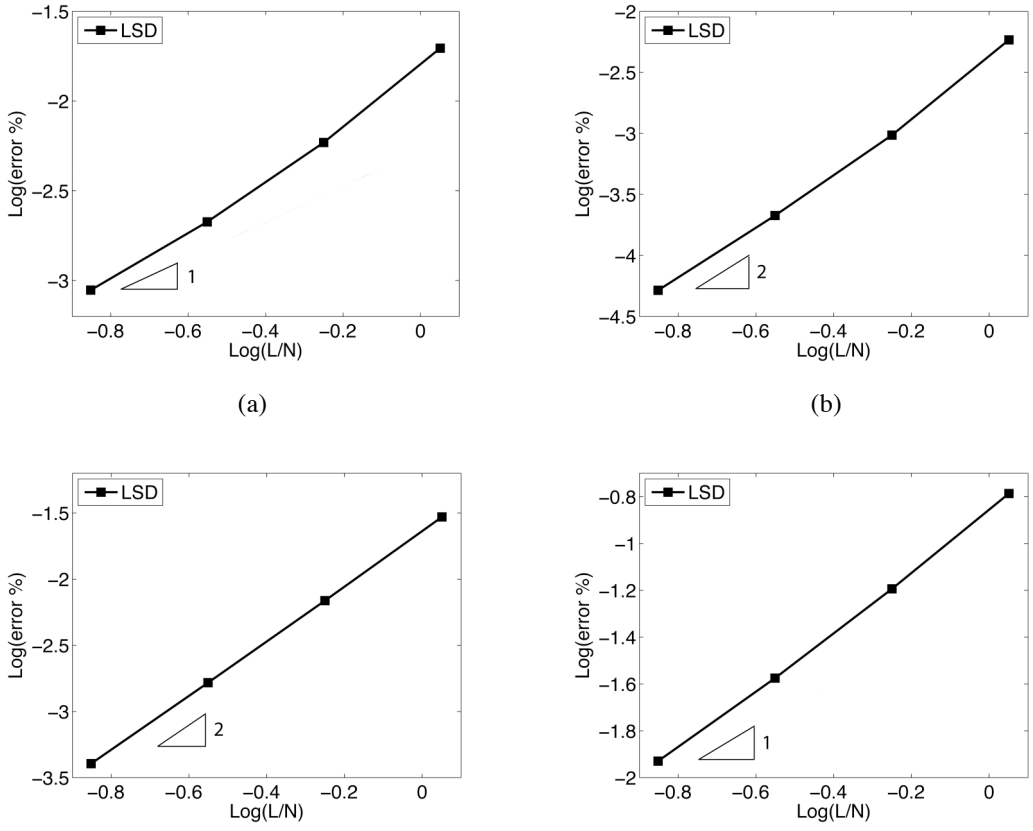

(a) (b)

(c) (d)

Fig 8.15 – Global convergence of stress profiles in (0/90/0). Global energy (a), in-plane stresses (b), transverse shear stresses (c) transverse normal stresses (d).

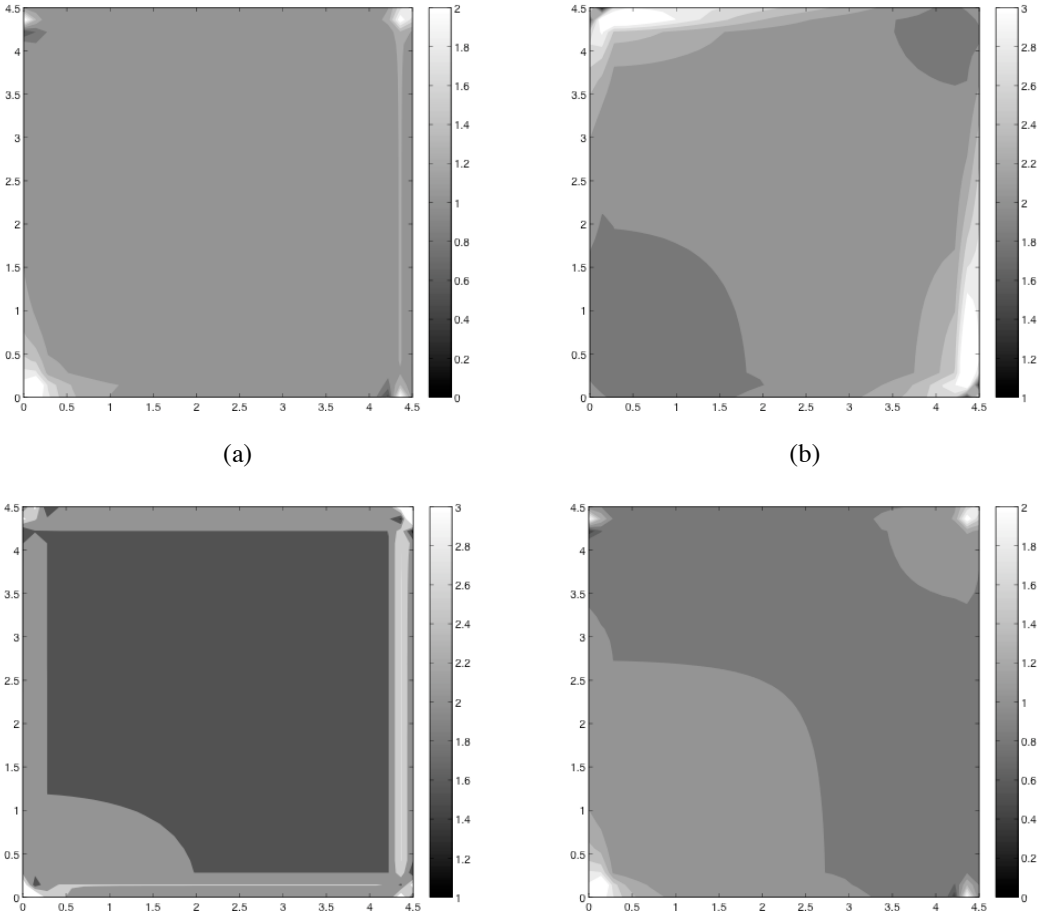

(a) (b)

(c) (d)

Fig 8.16 – Convergence map for (0/90/0). Global energy (a), in-plane stresses (b), transverse shear stresses (c), transverse normal stresses (d).

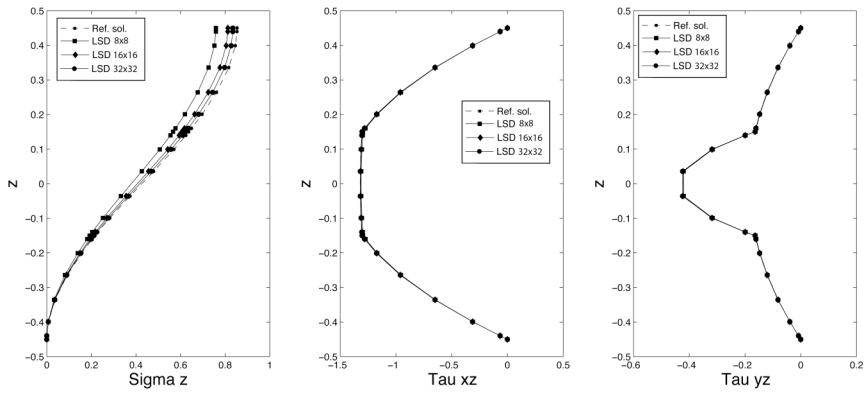

Fig 8.17 – Reconstructed transverse stress profiles at point A for (0/90/0) for different mesh refinements.

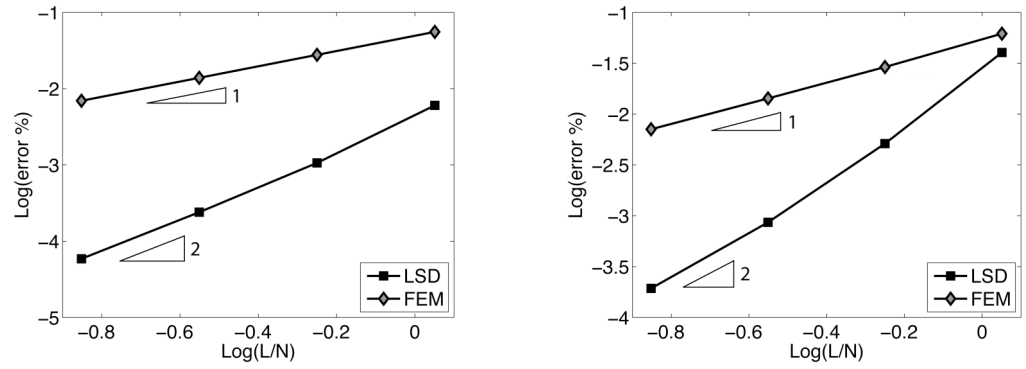

(a) (b)

Fig 8.18 – Global convergence of stress resultants for (0/90). Moments and membrane (a), Shear (b)

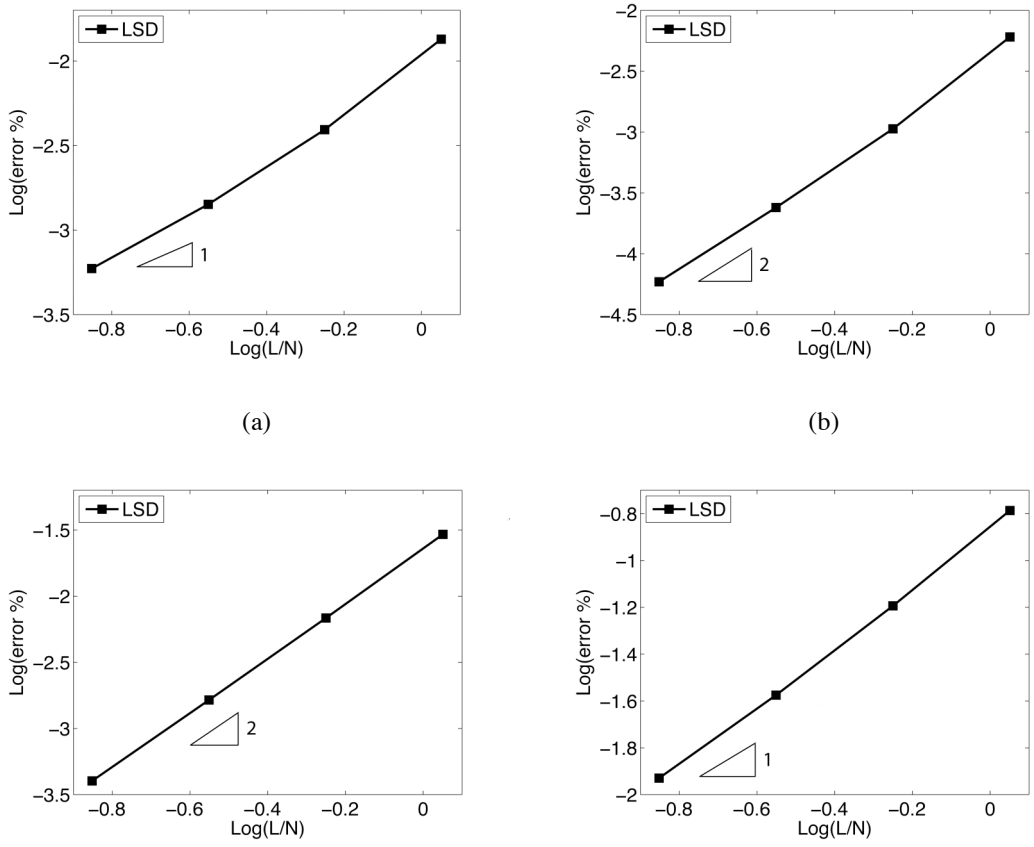

(a) (b)

(c) (d)

Fig 8.19 – Global convergence of stress profiles in (0/90). Global energy (a),, in-plane stresses (b), transverse shear stresses (c) transverse normal stresses (d).

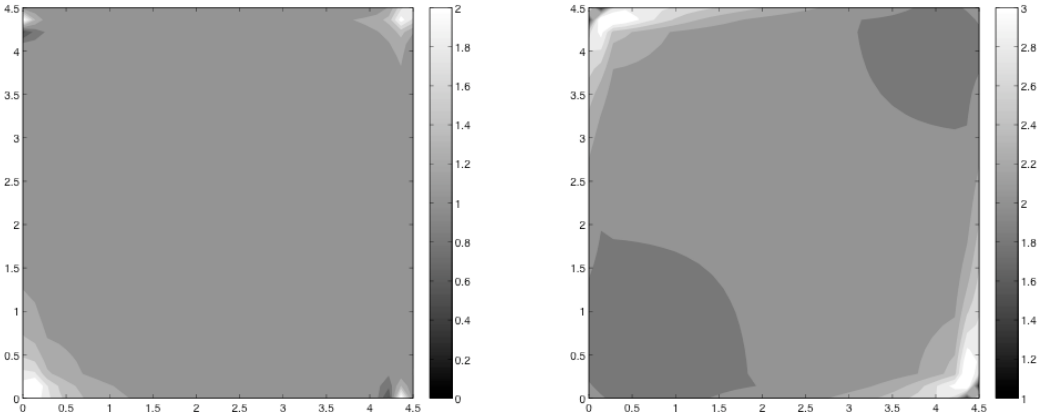

(a) (b)

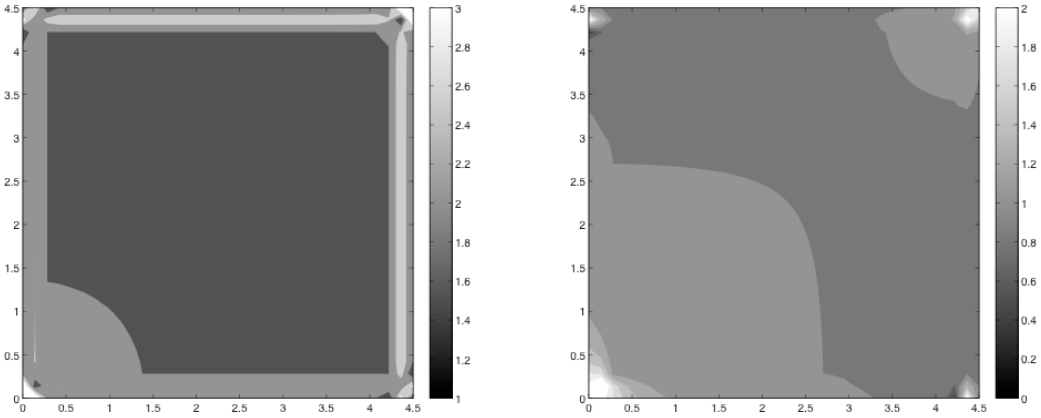

(c) (d)

Fig 8.20 – Convergence map for (0/90). Global energy (a), in-plane stresses (b), transverse shear stresses (c), transverse normal stresses (d).

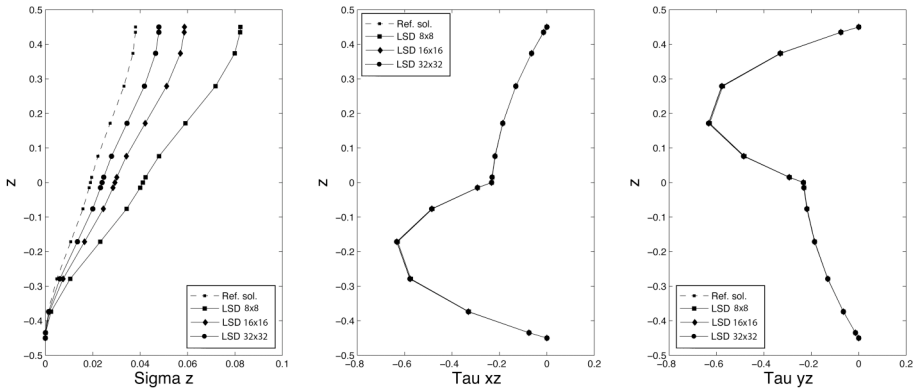

Fig 8.21 – Reconstructed transverse stress profiles at point B for (0/90) in an 8x8 mesh.

Conclusions

The present work focuses on stress recovery techniques aiming at obtaining a procedure that ensures convergence of stresses second order derivatives.

Enhanced stress fields can be used in several practical applications like automatic mesh refinement and transverse stress profile reconstruction in laminated plates. In the first case the enhanced stress field is used to calculate an error estimation in order to drive the refinement process while, in the second case, first and second order derivatives of stress resultants are used in order to reconstruct the transverse shear and normal stress profiles respectively using three-dimensional equilibrium equations.

It can be demonstrated that, if stresses satisfy pointwise equilibrium equations, the reconstruction procedure is extremely simple without any need of additional correction in order to meet boundary conditions on the top and bottom sides of the laminate.

Recovery by Compatibility in Patches (RCP) is here chosen to enhance stress fields due to its equilibrating nature and it is properly modified in order to ensure second order derivatives convergence and consequently of the whole transverse stress profile reconstruction strategy. Two different approaches and their combination are here analyzed: the first one is to perform a second recovery on recovered stresses and the second one is to consider larger patches.

Numerical tests in plain stress conditions are first presented showing the effectiveness of the proposed procedures and are used to confirm results later obtained for a bending problem in a laminated plate where the profile reconstruction is actually performed.

Afterwards, a new stress recovery procedure called Last Square Displacements (LSD), based on nodal displacement interpolation, is introduced and numerical results are presented. This new technique is extremely cost effective, it ensures convergence of stresses and their first and second order derivatives, is easily extendable to other physical fields and shows to be ultraconvergent.

Results concerning RCP show that considering larger patches, even though improve asymptotical convergence stability of stress derivatives, decreases their accuracy. On the other side, performing the double recovery ensures better accuracy but has a higher computational cost. Despite these differences, all RCP based procedures have shown very high accuracy for stresses and their first and second derivatives leading always to accurate reconstructed stress profiles probably also due to its equilibrating nature.

Last Square Displacements procedure shows to be extremely stable, cost effective and accurate in evaluating stresses and their first derivatives but poor accuracy is reached in evaluating second order derivatives leading to inaccurate transverse normal stress profiles.

It can be concluded that, on one hand, RCP on single patch with double recovery is the most suitable technique for transverse stress profile reconstruction as it is the best compromise between accuracy, convergence stability and computational cost. On the other hand, LSD is the most suitable for automatic mesh refinement as it has a minimal computational cost ensuring very high stress accuracy even at coarse mesh refinements.

For future research, two possibilities could be investigated. The first one is to develop a mixed technique introducing LSD stresses in RCP procedure. Stress fields enhanced by LSD could then undergo RCP element-by-element without the need of a patch based approach ensuring lower computational costs.

The second one is to add equilibrium constraint to LSD in order to obtain better performances. This would be possible imposing OLS minimization at the some time for all displacements field and adding conditions on derivatives in order to satisfy punctual equilibrium equations in selected points. This second possibility would increase the procedure computational cost but could ensure higher accuracy. In fact, adding equilibrium equations, it would be possible to use high order polynomial sets on small patches ensuring pseudoinverse matrix invertibility.

References

[1] O.C. Zienkiewicz, J.Z. Zhu A simple error estimator and adaptive procedure for practical engineering analysis. *International Journal for Numerical Methods in Engineering,* **24**, 1987, 337-357.

[2] B. Boroomand, O.C. Zienkiewicz, Recoveru by equilibrium in patches (REP), *International Journal for Numerical Methods in Engineering.* **40**, 1997, 137-154.

[3] F. Ubertini, 2004. Patch recovery based on complementary Energy. *International Journal for Numerical Methods in Engineering* **59**, 1501-1538.

[4] M.G. Vallet, C.M. Manole, J. Dompierre, S. Dufour, F. Guibault, Numerical comparison of some Hessian recovery techniques, *Int. J. Num. Meth. Engng.*. **72**, 987–1007, 2007.

[5] F. Daghia, S de Miranda, F Ubertini, E Viola A hybrid stress approach for laminated composite plates within the First-order Shear Deformation Theory, *Int. J. Solids and Struct.*, **45**, 1766-1787, 2008.

[6] G. Castellazzi, S. de Miranda, F. Ubertini, A posteriori error estimation in finite element analysis of plate structures. In: Proceedings of the Seventh World Congress on Computational Mechanics. WCCM VII, Lo Angeles, USA, 2006

[7] A. Benedetti, S. de Miranda F. Ubertini. A posteriori error estimation based on the superconvergent recovery by compatibility in patches. *International Journal for Numerical Methods in Engineering* **67**, 108-131.

[8] J.N. Reddy, Mechanics of Laminated Composite Plates-Theory and Analysis, CRC press, 1997.

[9] M. Laitienen, H. Lahtinen, S.G. Sjölind. Transverse shear correction factors for laminates in cylindrical bending. Communications in Numerical Methods in Engineering **11**, 41-47.